Photoreceptors generate neuronal diversity in their target field through a Hedgehog morphogen gradient in *Drosophila*

Matthew P. Bostock, Anadika R. Prasad, Alicia Donoghue, and Vilaiwan M. Fernandes*.

Department of Cell and Developmental Biology, University College London, Gower Street, London, WC1E 6BT.

*Corresponding author; vilaiwan.fernandes@ucl.ac.uk

Abstract:

Defining the origin of neuronal diversity is a major challenge in developmental neurobiology. The *Drosophila* visual system is an excellent paradigm to study how cellular diversity is generated. Photoreceptors from the eye disc grow their axons into the optic lobe and secrete Hedgehog (Hh) to induce the lamina, such that for every unit eye there is a corresponding lamina unit made up of post-mitotic precursors stacked into columns. Each differentiated column contains five lamina neuron types (L1-L5), making it the simplest neuropil in the optic lobe, yet how this diversity is generated was unknown. Here, we found that Hh pathway activity is graded along the distal-proximal axis of lamina columns and further determined that this gradient in pathway activity arises from a gradient of Hh ligand. We manipulated Hh pathway activity cell-autonomously in lamina precursors and non-cell autonomously by inactivating the Hh ligand, and by knocking it down in photoreceptors. These manipulations showed that different thresholds of activity specify unique cell identities, with more proximal cell types specified in response to progressively lower Hh levels. Thus, our data establish that Hh acts as a morphogen to pattern the lamina. Although, this is the first such report during *Drosophila* nervous system development, our work uncovers a remarkable similarity with the vertebrate neural tube, which is patterned by Sonic Hedgehog. Altogether, we show that differentiating neurons can regulate the neuronal diversity of their distant target fields through morphogen gradients.

Introduction:

Our nervous systems are composed of more unique cell types than any other organ. This diversity is believed to underlie our ability to process sensory input and perform complex specialized tasks. Invertebrates and vertebrates deploy common developmental strategies to diversify neural cell types (Holguera and Desplan, 2018). To explore these, we used the complex but tractable visual system of *Drosophila melanogaster,* which is organized into repeated modular circuits that map the visual field.

The *Drosophila* visual system is composed of the compound eyes and optic lobes, which together contain ~200 neuronal cell types (Fischbach and Dittrich, 1989; Kurmangaliyev et al., 2020; Özel et al., 2021). Each optic lobe is made up of four distinct neuropils, the lamina, medulla, lobula and lobula plate. With ~100 cell types, the medulla is the most diverse and complex (Fischbach and Dittrich, 1989; Özel et al., 2021). Despite this, work in recent years has uncovered that the interplay between spatial patterning, temporal patterning and Notch-mediated binary fate decisions accounts for medulla diversity (Bertet et al., 2014; Erclik et al., 2017; Gold and Brand, 2014; Konstantinides et al., 2021; Li et al., 2013). In contrast, much less is known about how diversity is generated in the arguably simpler lamina, which contains only 5 neuronal cell types (L1-L5).

The lamina is the first neuropil to receive input from the photoreceptors and its development is linked to and dependent on photoreceptor development (Huang et al., 1998; Huang and Kunes, 1998, 1996; Sugie et al., 2010; Umetsu et al., 2006; Yogev et al., 2010). Photoreceptors are born progressively in the wake of a wave of differentiation that sweeps across the eye disc (Figure 1A) (Roignant and Treisman, 2009). Two photoreceptor-derived signals, Hedgehog (Hh) and the Epidermal Growth Factor (EGF) Spitz, drive lamina development (Fernandes et al., 2017; Huang et al., 1998; Huang and Kunes, 1998, 1996; Sugie et al., 2010; Umetsu et al., 2006; Yogev et al., 2010). Hh signalling induces neuroepithelial cells to adopt lamina precursor cell (LPC) identity and express the lamina marker Dachshund (Dac). LPCs do not express classic neuroblast markers but are instead a distinct progenitor type, which undergo terminal divisions in response to Hh signalling (Apitz and Salecker, 2014). Finally, Hh signalling also promotes LPC adhesion to photoreceptor axons, which facilitates their assembly into columns (*i.e.* ensembles of stacked LPC cell bodies associated with photoreceptor axon bundles; Figure 1A, B) (Huang and Kunes, 1998, 1996; Sugie et al., 2010; Umetsu et al., 2006). Later in development, photoreceptor-derived EGF is required for LPCs to initiate neuronal differentiation (indicated by expression of the pan-neuronal marker Embryonic lethal abnormal vision [Elav]; Figure 1A, B) (Huang et al., 1998; Yogev et al., 2010); however, this communication is indirect and involves a signalling relay through multiple glial populations, which ultimately induce lamina neuron differentiation through Mitogen Activated Protein Kinase (MAPK) signalling (Figure 1A) (Fernandes et al., 2017; Prasad et al., 2021). Lamina neuron identities are invariant and stereotyped according to their position along the distal-proximal axis of columns; LPCs in the distal-most positions of columns will differentiate into L2s, followed by L3s, then L1s, then L4s, and finally L5s are positioned at the proximal end of columns (Figure 1A, C) (Pecot et al.,

2014). In addition, we can distinguish lamina neuron types using a combination of markers: Sloppy paired 2 (Slp2) alone labels L2s and L3s, Brain specific homeobox (Bsh) alone labels L4s, Seven up (Svp) together with Slp2 label L1s, and Slp2 together with Bsh label L5s (Figure 1A,C) (Pecot et al., 2014). The LPCs positioned between L4s and L5s do not differentiate but instead are fated to die by apoptosis (Figure 1A). Given that MAPK signalling drives differentiation in the lamina indiscriminately for all neuronal types (Fernandes et al., 2017; Prasad et al., 2021), how these neurons acquire their individual identities has remained elusive.

Here we showed that Hh signalling activity is graded from high to low along the distal-proximal axis of lamina columns. We examined the distribution of Hh ligand in the lamina and detected a protein gradient decreasing from a high point at the distal end of columns, consistent with the observed gradient of pathway activity. We then used genetic manipulations to modulate Hh signalling activity cell autonomously in LPCs or to disrupt Hh ligand directly and showed that different activity thresholds specify LPCs with distinct identities such that progressively decreasing Hh activity results in more and more proximal neuron identities being specified. These data establish that Hh is a morphogen in the lamina. Photoreceptors are the sole source of Hh to the optic lobes at these developmental stages (Huang and Kunes, 1996). We showed that Hh derived from photoreceptors patterns lamina cell identities, thus implying that in addition to inducing LPCs, promoting their assembly into columns and triggering their differentiation through glial signalling relays (Fernandes et al., 2017; Huang et al., 1998; Huang and Kunes, 1998, 1996; Prasad et al., 2021; Umetsu et al., 2006), photoreceptors also determine the neuronal diversity of the lamina. This is the first example of a morphogen patterning neuronal fates in *Drosophila*; it highlights a remarkable similarity with the ventral neural tube of vertebrates where a gradient of the morphogen Sonic Hedgehog, a Hh homologue, diversifies cell types (Placzek and Briscoe, 2018).

Results and Discussion:

Hh pathway activity is graded along the distal-proximal axis of LPC columns

For clues into how lamina neuron types are diversified, we integrated published single-cell RNA sequencing (scRNA-seq) datasets at developmental timepoints that span lamina development (Konstantinides et al., 2021; Kurmangaliyev et al., 2020; Özel et al., 2021) (Figure 1-figure supplement 1A; see Materials and Methods). As published previously, on uniform manifold approximation and projection (UMAP) visualizations L1, L2, L3 and L4 neuronal clusters were closer to each other than they were to the L5 cluster (Özel et al., 2021). The LPC cluster was connected to differentiated neurons by two streams of cells - one leading to the L1-L4 clusters and the other leading to the L5 cluster (Figure 1D); such convergent streams are thought to represent intermediate states between progenitors and differentiated cells (Konstantinides et al., 2021; Özel et al., 2021).

First, we probed these data to identify additional early markers of cell identity for each of the lamina neuron types (beyond Slp2, Bsh and Svp). Consistent with previous reports, scRNAseq analysis showed that L3 and L4 neurons expressed *earmuff (erm)* and *apterous (ap)*, respectively

(Tan et al., 2015; Ting et al., 2005). In addition, we found that *reduced ocelli (rdo)* was expressed at high levels in L2 neurons and at lower levels and more sporadically in L3 neurons, that L1 neurons expressed *Vesicular Glutamate transporter* (*VGlut) specifically,* and that L5 and L3 neurons expressed high and low levels of *defective proboscis extension response 8 (dpr8)*, respectively (Figure1-figure supplement 1B-F). We used *in situ* hybridisation chain reaction (HCR) (Choi et al., 2018) to validate marker expression *in vivo* at 0 hours after puparium formation (0h APF) (Figure 1- figure supplement 1G-K), thus providing additional markers for the differentiating lamina neuron types.

Next, we asked which transcripts distinguished L5 precursors from L1-L4 precursors during development in the scRNA-seq data (see Materials and Methods). Surprisingly, comparing gene expression between the two streams connecting undifferentiated LPCs with L1-L4s and L5s, indicated that several well-established Hh signalling targets were expressed at higher levels in the L1-L4 stream compared with the L5 stream, suggesting that L5 precursors experience lower Hh signalling than other lamina precursors. These included the direct transcriptional target *patched (ptc),* as well as *single-minded (sim), rhomboid (rho)* and *Zinc finger homeodomain 1 (zfh1)* (Figure 1E-H) (Albert et al., 2018; Biehs et al., 2010; Chen and Struhl, 1996; Umetsu et al., 2006). To validate these data *in vivo* we examined expression of a transcriptional reporter for *ptc (ptc-lacZ)* as a readout of Hh signalling activity (Chen and Struhl, 1996; Tabata and Kornberg, 1994) (Figure 1I). We measured the mean fluorescence intensity of β-Galactosidase (β-Gal) in the lamina at six cell positions corresponding to each LPC position within a column (*i.e.,* position 1 corresponded to the most distal cell (prospective L2) and position 6 corresponded to the most proximal cell (prospective L5) in columns; schematic in Figure 1J) from young to old columns (anterior to posterior axis). To do so we generated average intensity projections (from 10 optical slices) obtained from the central lamina and then measured the fluorescence intensity profiles for each of the 6 cell positions from the youngest column to the oldest column (quantified in Figure 1J with summary statistics from a mixed effects linear model in Table S1; see Materials and Methods for more detail). We also measured the mean fluorescence intensity of β-Gal for each cell along the distal to proximal axis for the youngest column (Figure 1K). Consistent with the transcriptomic data where *ptc* expression was lowest in older maturing neurons (Figure 1E), *ptc-lacZ* expression eventually decreased along the young to old axis for each of the six (distal-proximal) cell positions (Figure 1I,J; N=10). Importantly, in young columns prior to neuronal differentiation, we observed a gradient of *ptc-lacZ* expression, which was highest in the distal lamina and decreased along the distal-proximal axis (Figure 1K; one-way ANOVA with Dunn's multiple comparisons test, $P<0.0001$). Thus, we observed that the direct Hh signalling target, *ptc*, was graded along the distal to proximal length of the youngest column, indicating that there is a gradient of Hh signalling activity in lamina columns prior to neuronal differentiation.

Hh::GFP is distributed in a protein gradient in the lamina

We sought to determine if graded Hh pathway activity in the lamina arises from a concentration gradient of Hh ligand. We analysed the distribution of Hh protein tagged with superfolder GFP (Hh::GFP) expressed under the control of endogenous enhancers of the *hh* locus and inserted into the genome using a Bacterial Artificial Chromosome in single copy (Chen et al., 2017). This transgene was previously reported to rescue a *hh* amorph, indicating that it is a functional *hh* allele (Chen et al., 2017). We first used immunohistochemistry (IHC) to detect Hh::GFP and observed higher levels in younger photoreceptor cell bodies compared to older photoreceptor cell bodies in the eye disc, consistent with previous reports (Figure 2A) (Huang and Kunes, 1996). We also observed Hh::GFP in photoreceptor axons in the optic stalk, but observed very little signal in photoreceptor axons in the lamina (Figure 2A; N=18). Secreted proteins can be particularly sensitive to fixation and washes during IHC, therefore to avoid any confounding artefacts potentially caused by IHC, we visualised Hh::GFP live in cultured brain explants (Bostock et al., 2020) (Figure 2B). We measured Hh::GFP mean fluorescence intensity as a function of distal-proximal distance for the youngest lamina column (see Materials and Methods) and observed a gradient polarised from high to low from the distal to proximal ends of columns (Figure 2B-C; N=10). These measurements do not distinguish between intracellular and extracellular Hh::GFP, but instead represent total Hh::GFP. Nonetheless, these data indicate that Hh ligand is present in a distal-to-proximal gradient in the lamina, consistent with the gradient in Hh pathway activity along lamina columns and suggest that ligand availability is responsible for the activity gradient.

High and low extremes of Hh pathway activity cell-autonomously specify distal and proximal lamina neuron identities, respectively.

Hh signalling is known to trigger the early steps of lamina development, including promoting early lamina marker expression such as *dac* and *sim*, as well as promoting terminal LPC divisions and column assembly (Huang and Kunes, 1998, 1996; Sugie et al., 2010; Umetsu et al., 2006). However, no role for Hh in lamina neuron specification or differentiation has been identified thus far. In the vertebrate neural tube, a gradient of Sonic Hedgehog (Shh) signalling specifies ventral progenitor identities (Placzek and Briscoe, 2018), therefore, we wondered whether the graded Hh pathway activity we observed could specify neuronal identity in LPCs; in particular, we hypothesised that high Hh signalling levels in LPCs specify distal neuron identity (*i.e.* L2s) and low Hh signalling levels specify proximal neuron identity (*i.e.* L5s).

To test this, we asked whether increasing Hh signalling cell-autonomously would specify LPCs to differentiate with distal lamina neuron identity (*i.e.* L2). We generated LPCs with a gain-of-function in Hh pathway activity by inducing positively-labelled clones (Lee and Luo, 2001) that were homozygous mutant for the negative Hh pathway regulator *ptc* (Chen and Struhl, 1996; Kalderon, 2005). *ptc* mutant clones never contained L5s (Slp2 and Bsh co-expressing cells), L4s (Bsh-only expressing cells) or L1s (Svp and Slp2 co-expressing cells), but instead only contained neurons singly positive for Slp2, indicative of L2/L3 identity (Figure 3A-B; 17/17 clones from 15 optic lobes; fully penetrant phenotype). To determine the precise identity of these

neurons (L2 or L3), we examined expression of *rdo* and *erm* by HCR in *ptc* mutant clones in the proximal lamina and found mixed *rdo* and *erm* expression (Figure 3C-D; N=15/15 clones), which indicated that both L2 and L3 neurons were present in the clones. Thus, increasing Hh signalling maximally in the lamina resulted in distal neuron specification (mixed L2 and L3) at the expense of L1, L4 and L5 specification.

Next, we sought to disrupt Hh signalling cell autonomously in the lamina and assess the effects on lamina neuron specification. When we blocked Hh pathway activity completely in clones mutant for *smoothened (smo),* we did not recover any Dac-expressing LPCs (Figure 3-figure supplement 1A; N=15/15 clones; fully penetrant phenotype), consistent with previous reports (Huang and Kunes, 1998). Therefore, to reduce Hh pathway activity partially we used a lamina-specific driver (*R27G05-Gal4*), which drives expression in Dac-expressing LPCs exiting the posterior lamina furrow (Figure 3-figure supplement 1B), to express a repressor form of the transcriptional effector of Hh signalling, Cubitus interruptus (Ci; referred to as Ci^{rep}) (Busson and Pret, 2007). We used a temperature sensitive Gal80 ($Gal80^{ts}$) to restrict Gal4 activity temporally by raising crosses at the permissive temperature for $Gal80^{ts}$ and shifting to the restrictive temperature (29°C) to allow Gal4 activity from the third larval instar (see Materials and Methods). Expressing Ci^{rep} in LPCs led to a 2.8-fold increase in the proportion of Bsh and Slp2 double-positive L5s relative to controls, while the proportion of other lamina neuron subtypes was reduced relative to controls (Figure 3E,F,H-L and Figure 3-figure supplement 1C-F; one-way ANOVA with Dunn's multiple comparisons test; P-values<0.001; N=10). Moreover, whereas in control laminas L5s were only observed as a single row in the proximal lamina, expressing Ci^{rep} caused Bsh and Slp2 double-positive L5s to be distributed along the entire distal-proximal lengths of columns (Figure 3F, N=10). Similarly, knocking down Ci in the lamina by RNA interference (Ci^{RNAi}) (Figure 3G; N=9) resulted in ectopic L5s (2.4-fold increase relative to controls, one-way ANOVA with Dunn's multiple comparisons test; P<0.0001) and a reduction in the proportion of L2/L3s and L4 lamina neurons relative to controls (Figure 3H-L, one-way ANOVA with Dunn's multiple comparisons test; $P^{L2/L3}$<0.0001 and P^{L4}<0.0001; see Figure 3-figure supplement 1C-F for raw values). Thus, decreasing Hh signalling autonomously within LPCs was sufficient to induce the most proximal cell identity (L5s), throughout the distal-proximal lengths of columns and at the expense of other neuronal types. In summary, disrupting Hh signalling activity cell autonomously to either high or low extremes specified LPCs with either the most distal or proximal lamina neuron identities, respectively.

Intermediate levels of Hh signalling activity specify intermediate lamina neuron identities

The data presented thus far are consistent with Hh acting as a morphogen to specify cell identities in the lamina, *i.e.* in a concentration-dependent manner, however, our cell-autonomous manipulations only determined the impact of experiencing either the high or low extremes of pathway activity on lamina neuron identity specification. Therefore, we attempted to tune Hh signalling to intermediate levels by using the Gal4/UAS system to express Ci^{rep} in the lamina as before under two temperature conditions (in the presence of $Gal80^{ts}$): 29°C for a strong

inhibition of Hh signalling (as above) and 25°C for a milder inhibition. We then evaluated the distribution of lamina neuron types using *rdo, erm, VGlut, ap, dpr8* and *bsh.* Strong inhibition of Hh signalling (*lamina*^{ts}>*Ci*^{rep} at 29°C) led to a 2.2-fold increase relative to controls in the proportion of the lamina that co-expressed *dpr8* and *bsh* (*i.e.* L5s) at the expense of other markers (Figure 4A- F, J-N; $N^{dpr8+bsh}$=8; one-way ANOVA with Dunn's multiple comparisons test; $P^{dpr8+bsh}$<0.0001). As before, *dpr8* and *bsh* coexpressing cells (L5s) were no longer restricted to a single row in the proximal lamina but were distributed along the entire distal-proximal lengths of columns (Figure 4C,F). In contrast, milder inhibition of Hh signalling (*lamina*^{ts}>*Ci*^{rep} at 25°C) led to a 2.5-fold increase relative to controls in the proportion of the lamina that expressed *VGlut* (*i.e.* L1s), and a 1.9-fold increase relative to controls in the proportion of the lamina that expressed *ap* (*i.e.* L4s), at the expense of *rdo* expressing *(erm*-negative*)* L2s (Figure 4A-C, G-I, J-N; one-way ANOVA with Dunn's multiple comparisons test; P^{VGlut}<0.0001; P^{ap}<0.01). We obtained similar results when we evaluated the distribution of neuron types with Slp2, Svp and Bsh (Figure 4- figure supplement 1). Thus, intermediate neuron identities (L1s and L4s) were favoured when we tuned Hh signalling to intermediate levels.

To further test whether different thresholds of Hh ligand determine lamina neuron identities, we sought to manipulate Hh directly and to differing degrees of severity. We predicted that, if Hh was acting as a morphogen, progressively reducing Hh levels should result in progressively more proximal identities. To do so, we used animals harbouring a temperature sensitive loss of function allele of *hh (hh*^{ts2}*),* which we raised at the permissive temperature (18˚C) and then shifted to the restrictive temperature (29˚C) for either 6 hours, 12 hours, 24 hours, 45 hours or 72 hours before dissecting at the white prepupal stage (Figure 5A-G, Figure 5-figure supplement 1A-J). Consistent with the known role of Hh signalling in photoreceptor and early lamina development (Huang and Kunes, 1996), we recovered fewer and fewer photoreceptors and lamina neurons with increasing lengths of temperature shifts (Figure 5-figure supplement 1A-J), with no LPCs or lamina neurons recovered for the 45- and 72-hour temperature shifts (Figure 5F,G) (Huang and Kunes, 1996). These results indicated that our perturbations effectively titrated the availability of functional Hh with longer periods at the restrictive temperature. Next, we used lamina neuron type-specific markers to evaluate neuronal cell types under these conditions. We found that the proportion of L2/L3s (Slp2 single positive neurons) decreased as the availability of functional Hh was titrated to lower and lower levels, whereas the proportion of L5s (Slp2 and Bsh double-positive neurons) increased (Figure 5A-E; quantified in Figure 5I-L; one-way ANOVA with Dunn's multiple comparisons test; P-values<0.05). Importantly, the proportion of L1s (Slp2 and Svp double positive neurons) increased only for the 6-hour temperature shift. Thus, L1 neurons, which normally occupy intermediate lamina column positions were favoured at the expense of distal neuron types at intermediate thresholds of Hh pathway activity (Figure 5C, J; one-way ANOVA with Dunn's multiple comparisons test; P-values<0.05). Notably, under these conditions L1s and L5s were no longer confined to their normal positions within lamina columns but were observed throughout

(Figure 5A-D). Altogether our data establish that Hh acts as a morphogen to diversify lamina neuron types.

Photoreceptor-derived Hh specifies lamina neuron identities

Others have reported previously that photoreceptors are the sole source of Hh to the optic lobes during lamina development (Huang and Kunes, 1996). We corroborated these results using an enhancer trap in the *hh* locus *(hh-lacZ; hh^{P30}),* which showed that β-Gal expression was restricted to photoreceptors in the eye disc and absent from the optic lobes, except for a few sparse cells near the central brain (Figure 6A). We reasoned that if photoreceptor-derived Hh indeed patterns lamina neuron identities, then disrupting Hh expression specifically in photoreceptors should in turn result in lamina neuron patterning defects. Hh secreted by developing photoreceptors is required to drive morphogenetic furrow progression and continued photoreceptor development in the eye disc (Greenwood and Struhl, 1999; Treisman, 2013). Consequently, removing *hh* expression completely in the eye disc has been shown to block both photoreceptor development (Greenwood and Struhl, 1999; Treisman, 2013) and lamina development, due to its early role in inducing LPCs (Huang and Kunes, 1998, 1996). Therefore, we used *GMR-Gal4*, which is expressed after photoreceptor birth together with a previously validated RNAi line (Kim et al., 2014; Ni et al., 2011; Sahai-hernandez and Nystul, 2013) to partially knock down Hh in photoreceptors, thus bypassing its early roles. Under these conditions, lamina size was not noticeably affected, indicative of a mild knockdown (Figure 6B,C). When we evaluated lamina neuron type identities, we found that Slp2 and Svp expressing cells (L1s) increased by 1.2 fold relative to controls (Figure 6C; Mann-Whitney U test; $P<0.001$; $N=10$), consistent with more lamina precursor cells experiencing intermediate Hh signalling activity. Importantly, L1 neurons were no longer restricted to a single row at intermediate positions in columns but instead were recovered in more distal positions (Figure 6C). Thus, partially knocking down Hh expression in photoreceptors disrupted lamina neuron patterning in favour of more intermediate cell identities (L1s), consistent with mildly decreasing Hh signalling to more intermediate levels in the lamina.

Here we uncovered a previously unknown role for Hh as a morphogen that specifies lamina neuron identities, thus revealing yet another layer of dependence of lamina development on photoreceptor-derived signals. Intriguingly, a mix of L2 and L3 identities were specified when Hh signalling was activated to maximum physiological levels (Figure 3D). This suggests that in addition to high Hh signalling levels, additional signals are required to further differentiate L2 from L3 identities. This is the first report of a morphogen patterning neuronal fates in *Drosophila*. It highlights the remarkable evolutionary conservation of this developmental strategy, which is widespread in vertebrates (Placzek and Briscoe, 2018; Sagner and Briscoe, 2019).

Nonetheless, it is not obvious how the Hh gradient is established in the lamina, such that it is polarised from high to low along the distal-proximal lengths of lamina columns, as

photoreceptor axons themselves span this full distance. Axonal trafficking of Hh was shown to be regulated by an evolutionarily conserved motif in its cleaved C-terminal domain (Chu et al., 2006; Daniele et al., 2017), disruption of which affected neuronal diversity in the lamina specifically (Chu et al., 2006). This indicates that axonal trafficking may play a role in establishing the Hh gradient, however, more work is required to uncover the exact molecular mechanisms involved. It is unexpected that neurons, here photoreceptors, define the neuronal diversity of their target field, and raises the possibility that neurons in other contexts could also be patterning their target fields during development through morphogen gradients. Indeed, many vertebrate neuronal types express Shh (Dakubo et al., 2003; Farmer et al., 2016; Garcia et al., 2010; Gonzalez-Reyes et al., 2012; Harwell et al., 2012; Petralia et al., 2011; Wallace, 1999), however, their ability to generate instructive gradients to pattern distant neural fields has not been determined thus far.

References

Albert EA, Puretskaia OA, Terekhanova N V, Labudina A. 2018. Direct control of somatic stem cell proliferation factors by the Drosophila testis stem cell niche **145**:dev156315. doi:10.1242/dev.156315

Apitz H, Salecker I. 2014. A challenge of numbers and diversity: neurogenesis in the Drosophila optic lobe. *J Neurogenet* **28**:1–35. doi:10.3109/01677063.2014.922558

Bertet C, Li X, Erclik T, Cavey M, Wells B, Desplan C. 2014. Temporal Patterning of Neuroblasts Controls Notch-Mediated Cell Survival through Regulation of Hid or Reaper. *Cell* **158**:1173–1186. doi:10.1016/j.cell.2014.07.045

Biehs B, Kechris K, Liu S, Kornberg TB. 2010. Hedgehog targets in the Drosophila embryo and the mechanisms that generate tissue-specific outputs of Hedgehog signaling. *Development* **137**:3887–3898. doi:10.1242/dev.055871

Bostock MP, Prasad AR, Chaouni R, Yuen AC, Sousa-Nunes R, Amoyel M, Fernandes VM. 2020. An immobilization technique for long-term time-lapse imaging of explanted Drosophila tissues. *Front Cell Dev Biol* **8**:1074. doi:10.3389/fcell.2020.590094

Busson D, Pret A. 2007. GAL4/UAS Targeted Gene Expression for Studying Drosophila Hedgehog Signaling. *Methods Mol Biol* **397**:161–201.

Chen W, Huang H, Hatori R, Kornberg TB. 2017. Essential basal cytonemes take up Hedgehog in the Drosophila wing imaginal disc. *Development* **144**:3134–3144.

Chen Y, Struhl G. 1996. Dual Roles for Patched in Sequestering and Transducing Hedgehog. *Cell* **87**:553–563.

Choi HMT, Schwarzkopf M, Fornace ME, Acharya A, Artavanis G, Stegmaier J, Cunha A, Pierce NA. 2018. Third-generation in situ hybridization chain reaction : multiplexed, quantitative, sensitive, versatile, robust. *Development* **145**:dev165753. doi:10.1242/dev.165753

Chotard C, Leung W, Salecker I. 2005. glial cells missing and gcm2 cell autonomously regulate both glial and neuronal development in the visual system of Drosophila. *Neuron* **48**:237–251. doi:10.1016/j.neuron.2005.09.019

Chu T, Chiu M, Zhang E, Kunes S. 2006. A C-Terminal Motif Targets Hedgehog to Axons, Coordinating Assembly of the Drosophila Eye and Brain. *Dev Cell* **10**:635–646.

Dakubo GD, Wang YP, Mazerolle C, Campsall K, Mcmahon AP, Wallace VA. 2003. Retinal

ganglion cell-derived Sonic Hedgehog signaling is required for optic disc and stalk neuroepithelial cell development. *Development* **130**:2967–2980.

Daniele JR, Chu T, Kunes S. 2017. A novel proteolytic event controls Hedgehog intracellular sorting and distribution to receptive fields. *Biol Open* **6**:540–550.

Erclik T, Li X, Courgeon M, Bertet C, Chen Z, Baumert R, Ng J, Koo C, Arain U, Behnia R, Del A, Rodriguez V, Senderowicz L, Negre N, Kevin P. 2017. Integration of temporal and spatial patterning generates neural diversity. *Nat Publ Gr* **541**:365–370. doi:10.1038/nature20794

Farmer WT, Abrahamsson T, Chierzi S, Lui C, Zaelzer C, Jones E, Ponroy Bally B, Chen GG, Theroux J-F, Pend J, Bourque CW, Charron F, Ernst C, Sjöström J, Murai KK. 2016. Neurons diversify astrocytes in the adult brain through sonic hedgehog signaling. *Science (80-)* **351**:849–854.

Fernandes VM, Chen Z, Rossi AM, Zipfel J, Desplan C. 2017. Glia relay differentiation cues to coordinate neuronal development in Drosophila. *Science (80-)* **357**:886–891.

Fischbach KF, Dittrich APM. 1989. The optic lobe of Drosophila melanogaster. I: A. Golgi analysis of wild-type structure. *Cell Tissue Res* **258**:441–475. doi:doi: 10.1007/BF00218858

Garcia ADR, Petrova R, Eng L, Joyner AL. 2010. Sonic Hedgehog regulates discrete populations of astrocytes in the adult mouse forebrain. *J Neurosci* **30**:13597–13608. doi:10.1523/JNEUROSCI.0830-10.2010

Gold KS, Brand AH. 2014. Optix defines a neuroepithelial compartment in the optic lobe of the Drosophila brain Optix defines a neuroepithelial compartment in the optic lobe of the Drosophila brain. *Neural Dev* **9**:18.

Gonzalez-Reyes LE, Verbitsky M, Blesa J, Jackson-lewis V, Paredes D, Tillack K, Phani S, Kramer ER, Przedborski S, Kottmann AH. 2012. Sonic Hedgehog Maintains Cellular in the Adult Nigrostriatal Circuit. *Neuron* **75**:306–319.

Greenwood S, Struhl G. 1999. Progression of the morphogenetic furrow in the Drosophila eye: the roles of Hedgehog, Decapentaplegic and the Raf pathway. *Development* **126**:5795–5808. doi:10.1242/DEV.126.24.5795

Guillermin O, Perruchoud B, Sprecher SG, Egger B. 2015. Characterization of Tailless functions during drosophila optic lobe formation. *Dev Biol* **405**:202–213. doi:10.1016/j.ydbio.2015.06.011

Harwell CC, Parker PRL, Gee SM, Okada A, Mcconnell SK, Kreitzer AC. 2012. Sonic Hedgehog Expression in Corticofugal Projection Neurons Directs Cortical Microcircuit Formation. *Neuron* **73**:1116–1126. doi:10.1016/j.neuron.2012.02.009

Hasegawa E, Kaido M, Takayama R, Sato M. 2013. Brain-specific-homeobox is required for the specification of neuronal types in the Drosophila optic lobe. *Dev Biol* **377**:90–99. doi:10.1016/j.ydbio.2013.02.012

Holguera I, Desplan C. 2018. Neuronal specification in space and time. *Science (80-)* **362**:176–180.

Huang Z, Kunes S. 1998. Signals transmitted along retinal axons in Drosophila: Hedgehog signal reception and the cell circuitry of lamina cartridge assembly. *Development* **125**:3753–64. doi:10.1016/s0092-8674(00)80094-x

Huang Z, Kunes S. 1996. Hedgehog, transmitted along retinal axons, triggers neurogenesis in the developing visual centers of the Drosophila brain. *Cell* **86**:411–22. doi:10.1016/S0092-8674(00)80114-2

Huang Z, Shilo BZ, Kunes S. 1998. A retinal axon fascicle uses spitz, an EGF receptor ligand, to

construct a synaptic cartridge in the brain of Drosophila. *Cell* **95**:693–703. doi:10.1016/S0092-8674(00)81639-6

Kalderon D. 2005. The mechanism of hedgehog signal transduction. *Biochem Soc Trans* **33**:1509–1512. doi:10.1042/BST0331509

Kim K, Vinayagam A, Perrimon N. 2014. A Rapid Genome-wide MicroRNA Screen Identifies miR-14 as a Modulator of Hedgehog Signaling. *Cell Rep* **7**:2066–2077. doi:10.1016/j.celrep.2014.05.025

Konstantinides N, Holguera I, Rossi AM, Escobar A, Dudragne L, Chen Y, Tran TN, Jaimes AMM, Özel MN, Simon F, Shao Z, Tsankova NM, Fullard JF. 2022. A complete temporal transcription factor series in the fly visual system. *Nature* **604**:316–322. doi:10.1038/s41586-022-04564-w

Konstantinides N, Rossi AM, Escobar A, Dudragne L, Chen Y-C, Tran T, Martinez A, Özel MN, Simon F, Shao Z, Nadejda M, Fullard JF, Walldorf U, Roussos P, Konstantinides N, Jaimes AM, Özel MN, Simon F, Shao Z, Tsankova NM, Fullard JF, Walldorf U, Roussos P, Desplan C. 2021. A comprehensive series of temporal transcription factors in the fly visual system. *bioRxiv* **06**:2021.06.13.448242.

Kurmangaliyev YZ, Yoo J, Valdes-aleman J, Sanfilippo P, Zipursky SL, Kurmangaliyev YZ, Yoo J, Valdes-aleman J, Sanfilippo P, Zipursky SL. 2020. Transcriptional Programs of Circuit Assembly in the Drosophila Visual System. *Neuron* **108**:1045–1057. doi:10.1016/j.neuron.2020.10.006

Lee T, Luo L. 2001. Mosaic analysis with a repressible cell marker (MARCM) for Drosophila neural development. *Trends Neurosci* **24**:251–4.

Li X, Chen Z, Desplan C. 2013. Temporal patterning of neural progenitors in drosophila, 1st ed, Current Topics in Developmental Biology. Elsevier Inc. doi:10.1016/B978-0-12-396968-2.00003-8

Ni J, Zhou R, Czech B, Liu L, Holderbaum L, Yang-zhou D, Shim H, Tao R, Handler D, Karpowicz P, Binari R, Booker M, Brennecke J, Perkins LA, Hannon GJ, Perrimon N. 2011. A genome-scale shRNA resource for transgenic RNAi in Drosophila. *Nat Methods* **8**:405–407. doi:10.1038/nmeth.1592

Özel MN, Simon F, Jafari S, Holguera I, Chen Y, Benhra N, El-danaf RN, Kapuralin K, Malin JA, Konstantinides N, Desplan C. 2021. Neuronal diversity and convergence in a visual system developmental atlas. *Nature* **589**:88–95. doi:10.1038/s41586-020-2879-3

Pecot M, Chen Y, Akin O, Chen Z, Tsui CYK, Zipursky SL. 2014. Sequential axon-derived signals couple target survival and layer specificity in the drosophila visual system. *Neuron* **82**:320–333. doi:10.1016/j.neuron.2014.02.045

Petralia RS, Wang Y, Mattson MP, Yao PJ, Petralia RS, Wang Y, Mattson MP, Yao PJ. 2011. Sonic hedgehog distribution within mature hippocampal neurons. *Comun Integr Biol* **4**:775–777. doi:10.4161/cib.17832

Piñeiro C, Lopes CS, Casares F. 2014. A conserved transcriptional network regulates lamina development in the Drosophila visual system. *Development* **141**:2838–47. doi:10.1242/dev.108670

Placzek M, Briscoe J. 2018. Sonic hedgehog in vertebrate neural tube development. *Int J Dev Biol* **62**:225–234.

Prasad AR, Lago-Baldaia I, Bostock MP, Housseini Z, Fernandes VM. 2021. Differentiation signals from glia are fine-tuned to set neuronal numbers during development. *bioRxiv* **2021.12.13**.

Roignant J-Y, Treisman JE. 2009. Pattern formation in the Drosophila eye disc. *Int J Dev Biol* **53**:795–804. doi:10.1387/ijdb.072483jr

Sagner A, Briscoe J. 2019. Establishing neuronal diversity in the spinal cord : a time and a place. *Development* **146**:dev182154. doi:10.1242/dev.182154

Sahai-hernandez P, Nystul TG. 2013. A dynamic population of stromal cells contributes to the follicle stem cell niche in the Drosophila ovary. *Development* **140**:4490–4498. doi:10.1242/dev.098558

Schindelin J, Arganda-carreras I, Frise E, Kaynig V, Longair M, Pietzsch T, Preibisch S, Rueden C, Saalfeld S, Schmid B, Tinevez J, White DJ, Hartenstein V, Eliceiri K, Tomancak P, Cardona A. 2012. Fiji : an open-source platform for biological-image analysis. *Nat Methods* **9**:676–682. doi:10.1038/nmeth.2019

Stuart T, Butler A, Hoffman P, Stoeckius M, Smibert P, Satija R, Stuart T, Butler A, Hoffman P, Hafemeister C, Papalexi E, Iii WMM, Hao Y, Stoeckius M, Smibert P, Satija R. 2019. Comprehensive Integration of Single-Cell Data Resource Comprehensive Integration of Single-Cell Data. *Cell* **177**:1888-1902.e21. doi:10.1016/j.cell.2019.05.031

Sugie A, Umetsu D, Yasugi T, Fischbach KF, Tabata T. 2010. Recognition of pre- and postsynaptic neurons via nephrin/NEPH1 homologs is a basis for the formation of the Drosophila retinotopic map. *Development* **137**:3303–3313. doi:10.1242/dev.047332

Tabata T, Kornberg TB. 1994. Hedgehog is a signaling protein with a key role in patterning Drosophila imaginal discs. *Cell* **76**:89–102.

Tan L, Zhang KX, Pecot MY, Nagarkar-Jaiswal S, Lee PT, Takemura SY, McEwen JM, Nern A, Xu S, Tadros W, Chen Z, Zinn K, Bellen HJ, Morey M, Zipursky SL. 2015. Ig Superfamily Ligand and Receptor Pairs Expressed in Synaptic Partners in Drosophila. *Cell* **163**:1756–1769. doi:10.1016/j.cell.2015.11.021

Ting C, Yonekura S, Chung P, Hsu S, Robertson HM, Chiba A, Lee C. 2005. Drosophila N-cadherin functions in the first stage of the two-stage layer-selection process of R7 photoreceptor afferents. *Development* **132**:953–963. doi:10.1242/dev.01661

Treisman JE. 2013. Retinal differentiation in Drosophila. *Wiley Interdiscip Rev Dev Biol* **2**:545–557. doi:10.1002/wdev.100

Umetsu D, Murakami S, Sato M, Tabata T. 2006. The highly ordered assembly of retinal axons and their synaptic partners is regulated by Hedgehog/Single-minded in the Drosophila visual system. *Development* **133**:791–800. doi:10.1242/dev.02253

Wallace VA. 1999. Purkinje-cell-derived Sonic hedgehog regulates granule neuron precursor cell proliferation in the developing mouse cerebellum. *Curr Biol* **9**:445–448.

Yogev S, Schejter ED, Shilo BZ. 2010. Polarized secretion of drosophila EGFR ligand from photoreceptor neurons is controlled by ER localization of the ligand-processing machinery. *PLoS Biol* **8**:e1000505.

Acknowledgements:

We thank C. Desplan, D. Kalderon, B. Shilo, G. Struhl and J. Treisman for reagents, and S. Ackerman, M. Amoyel, B. Conradt, C. Desplan, A. Franz, P. Salinas, A. Rossi, C. Stern, L. Venkatasubramanian and members of the Fernandes lab for comments on the manuscript. Stocks obtained from the Bloomington Drosophila Stock Center (NIH P40OD018537) were used in this study. Monoclonal antibodies obtained from the Developmental Studies Hybridoma Bank, created by the NICHD of the NIH and maintained at The University of Iowa, were used in this study.

Competing interests:
Authors declare that they have no competing interests.

Funding:
Wellcome Trust Sir Henry Dale Research Fellowship to VMF (210472/Z/18/Z), UCL Biosciences Graduate Research Scholarship to MPB, UCL Overseas Research Scholarship and UCL Graduate Research Scholarship to ARP, and UCL Research Opportunities Scholarship to AD.

Author contributions:
Conceptualization: VMF, MPB
Investigation: MPB
Supervision: VMF
Writing – original draft: VMF
Writing – review & editing: MPB, VMF
Revisions: VMF, MPB, ARP, AD

Figure 1

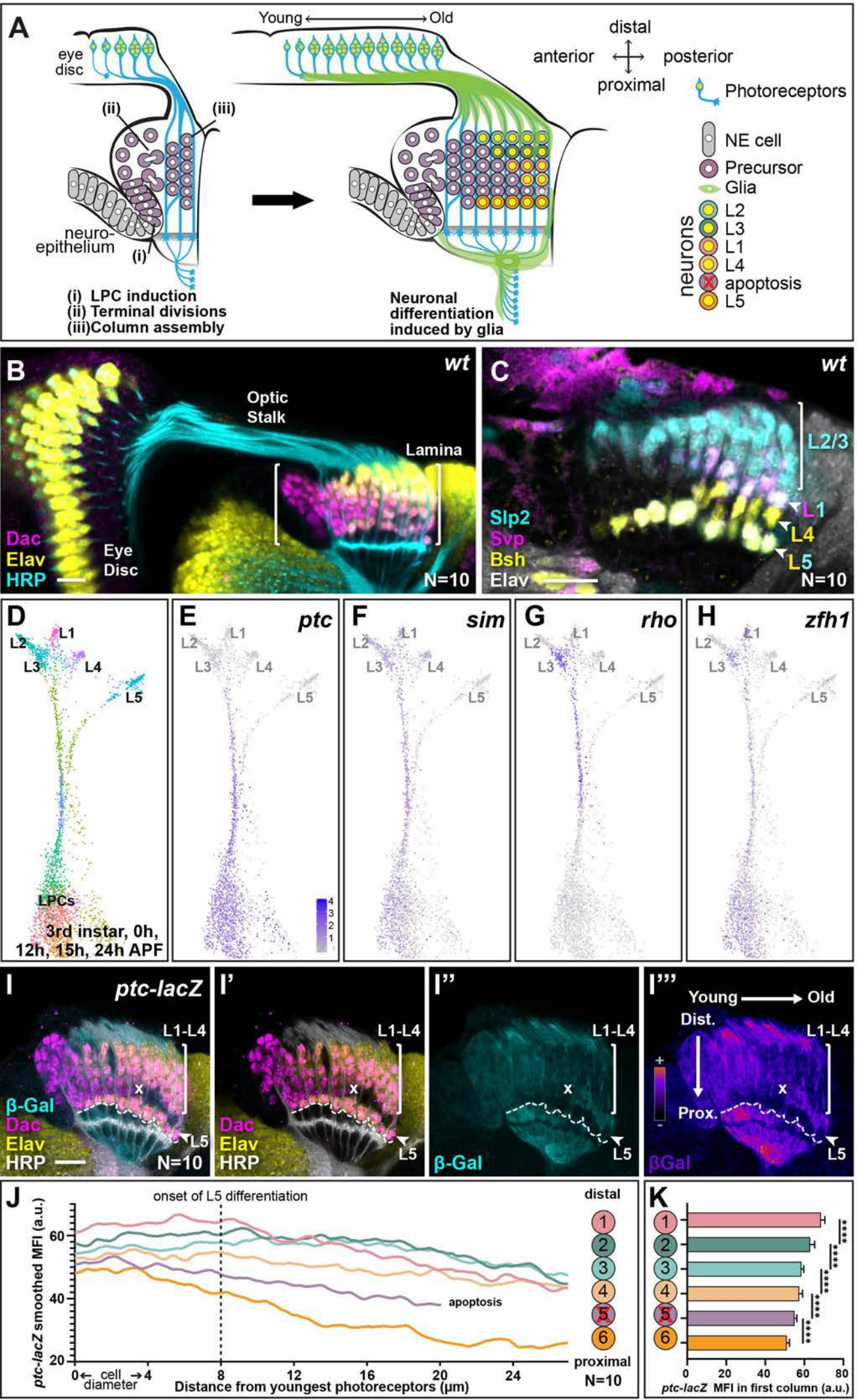
A
Young
Old
eye disc
(ii)
(iii)
neuro-epithelium
(i)
(i) LPC induction
(ii) Terminal divisions
(iii)Column assembly
Neuronal differentiation induced by glia
distal
anterior
posterior
proximal
Photoreceptors
NE cell
Precursor
Glia
neurons
L2
L3
L1
L4
apoptosis
L5
B
wt
Optic Stalk
Lamina
Dac
Elav
HRP
Eye Disc
N=10
C
wt
L2/3
L1
L4
L5
Slp2
Svp
Bsh
Elav
N=10
D
L1
L2
L3
L4
L5
LPCs
3rd instar, 0h, 12h, 15h, 24h APF
E
ptc
F
sim
G
rho
H
zfh1
I
ptc-lacZ
L1-L4
β-Gal
Dac
Elav
HRP
L5
N=10
I'
L1-L4
Dac
Elav
HRP
L5
I''
L1-L4
β-Gal
L5
I'''
Young
Old
Dist.
Prox.
L1-L4
βGal
L5
J
onset of L5 differentiation
ptc-lacZ smoothed MFI (a.u.)
apoptosis
cell diameter
Distance from youngest photoreceptors (μm)
distal
proximal
N=10
K
ptc-lacZ MFI in first column (a.u.)

Figure 1: Hh pathway activity is graded along lamina columns.
(A) Schematic of the developing lamina. Photoreceptor axons release Hh into the optic lobe which guides lamina development by driving neuroepithelial cells to develop into lamina precursor cells (LPCs), their terminal divisions and column assembly. Once assembled into columns of six LPCs each, LPCs differentiate into five distinct neuron types (L1-L5) in response to MAPK activity that is induced by signals from glia (Fernandes et al., 2017; Prasad et al., 2021). Lamina neuron types are positioned stereotypically along the distal to proximal axis of columns: L2, L3, L1, L4, L5; the LPCs between L4s and L5s undergo apoptosis. **(B)** A wildtype optic lobe and eye disc, with the developing lamina labelled by Dac (magenta), differentiating neurons by Elav (yellow) and photoreceptor axons by Horse Radish Peroxidase (HRP, cyan).
(C) A wildtype lamina labelled with lamina neuron-type-specific markers, Slp2 (cyan), Bsh (yellow), and Svp (magenta); all neurons are marked by Elav (white). Slp2 alone labels L2s and L3s, Bsh alone labels L4s, Svp together with Slp2 label L1s, and Slp2 together with Bsh label L5s. **(D)** UMAP visualisation of LPCs, differentiated L1-L5 neurons and intermediate stages of differentiation using 150 principal components calculated on the log-normalized integrated gene expression from single-cell RNA sequencing datasets of the third larval instar, 0 hours-, 12 hours-, 15 hours- and 24 hours-APF. See Figure 1-figure supplement 1A for full integrated dataset. **(E-H)** UMAP visualisation from (D; grey) showing log normalised expression of Hh signalling targets (blue): **(E)** *ptc*, **(F)**, *sim*, **(G)** *rho* and **(H)** *zfh1,* which all show higher levels of expression in the convergent stream connecting the LPC cluster with mature L1-L4 neuron clusters rather than the stream connecting the LPC cluster with the L5 neuron cluster.
(I) An optic lobe expressing *ptc-LacZ* stained for β-Galactosidase (β-Gal; cyan), Dac (magenta), Elav (yellow) and HRP (white). The two axes – young to old and proximal to distal are indicated in I''. (I''') shows (I'') in pseudo-colour. Dashed line marks the most proximal surface of the lamina. "x" marks the point from which the excess LPCs have been cleared.
(J) Smoothed (second order with 6 neighbours; see Materials and methods) mean fluorescence intensities (MFIs; arbitrary units; a.u.) of *ptc-LacZ* (β-Gal) by distal to proximal cell position as indicated. L5s and the excess LPCs began with and maintained the lowest levels of β-Gal expression over time. Summary statistics for the raw data in Table S1. **(K)** Same data as J plotted for the youngest lamina column only. Asterisks indicate significance: P-values<0.0001 from a one-way ANOVA with Dunn's multiple comparisons test. Scale bar = 20μm. See also Figure 1-figure supplement 1.

Figure 1 - figure supplement 1

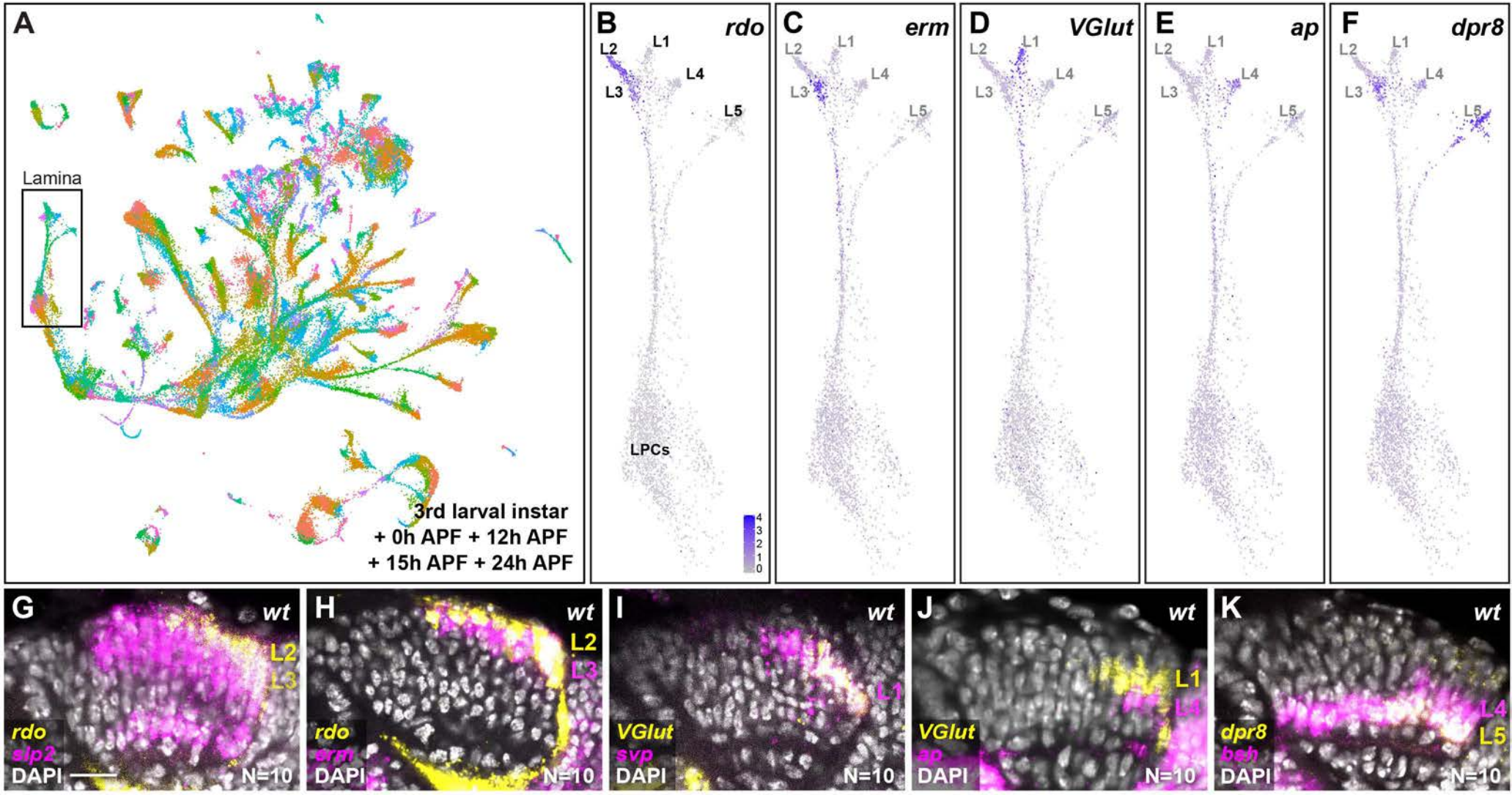

Figure 1-figure supplement 1: Identifying and validating additional lamina neuron type markers

(A) UMAP visualisation of integrated third larval instar, 0 hours-, 12 hours-, 15 hours- and 24 hours-APF single cell RNA sequencing datasets (Konstantinides et al., 2021; Kurmangaliyev et al., 2020; Özel et al., 2021) using 150 principal components calculated on the log-normalized integrated gene expression. Rectangle marks LPCs and lamina neurons of varying maturity, which were identified based on known markers and existing annotations from the 15h APF dataset as described in Materials and Methods. **(B-F)** UMAP of lamina cells from Figure 1D showing log normalised expression of the lamina neuron subtype markers (blue): **(B)** *rdo*, **(C)**, *erm*, **(D)** *Vglut* **(E)** *ap* and **(F)** *dpr8*. **(G-K)** *In situ* HCR for **(G)** *rdo* and *slp2*, **(H)**, *rdo* and *erm*, **(I)** *Vglut* and *svp,* **(J)** *Vglut* and *ap,* and **(K)** *dpr8* and *bsh* in the lamina at 0h APF using DAPI to mark all nuclei (white). Scale bar = 20µm.

Figure 2

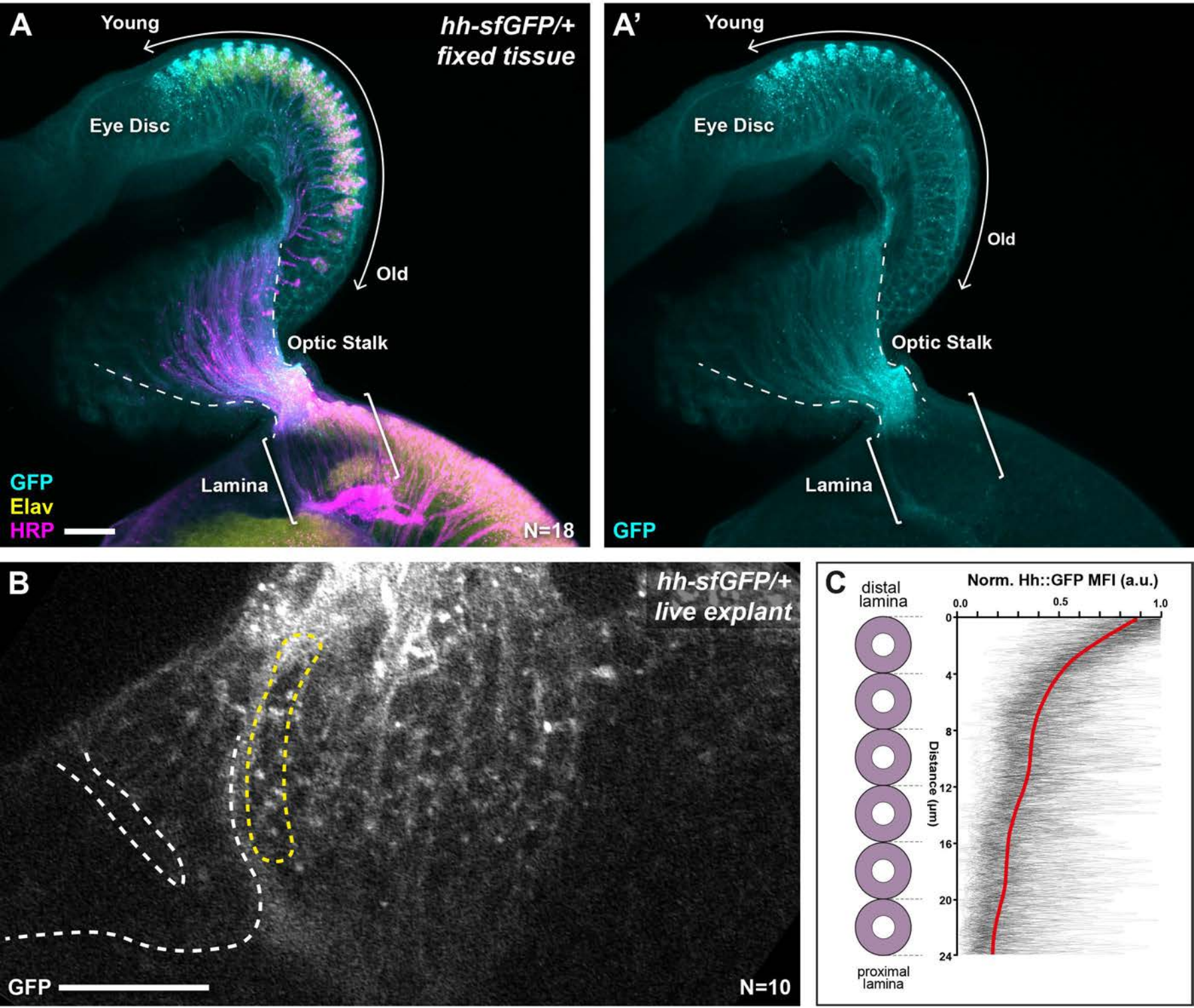
A
Young
hh-sfGFP/+
fixed tissue
Eye Disc
Old
Optic Stalk
Lamina
GFP
Elav
HRP
N=18
A'
Young
Eye Disc
Old
Optic Stalk
Lamina
GFP
B
hh-sfGFP/+
live explant
GFP
N=10
C
distal lamina
proximal lamina
Norm. Hh::GFP MFI (a.u.)
0.0
0.5
1.0
Distance (µm)
0
4
8
12
16
20
24

Figure 2: Hh::GFP is distributed in a protein gradient in the lamina.
(A) A maximum intensity projection of a *hh-sfGFP/+* optic lobe and eye disc complex (fixed tissue). Hh::GFP (cyan) detected by immunohistochemistry was present in photoreceptor cell bodies in the eye disc (Elav, yellow), with higher levels in younger photoreceptors as reported previously (Huang and Kunes, 1996) and photoreceptor axons in the optic stalk (HRP; magenta). Hh::GFP expression decreased rapidly once photoreceptors entered the lamina (brackets). **(B)** A cross-sectional view of the lamina from a live explant of *hh-sfGFP/+*. Hh::GFP puncta were visible more prominently in the distal lamina, with fewer and smaller puncta appearing in proximal regions. White dashed lines mark the lamina furrow. Yellow dashed line marks the youngest column. **(C)** Hh::GFP mean fluorescence intensity (MFI) plots from live explants normalised to the maximum MFI value for each plot (arbitrary units; a.u.) as a function of distance from distal to proximal cell position as indicated for the youngest lamina column (yellow dashed outline in B). The red line shows regression averaging of each of the MFI profiles (see Materials and Methods). Scale bar = 20µm.

Figure 3

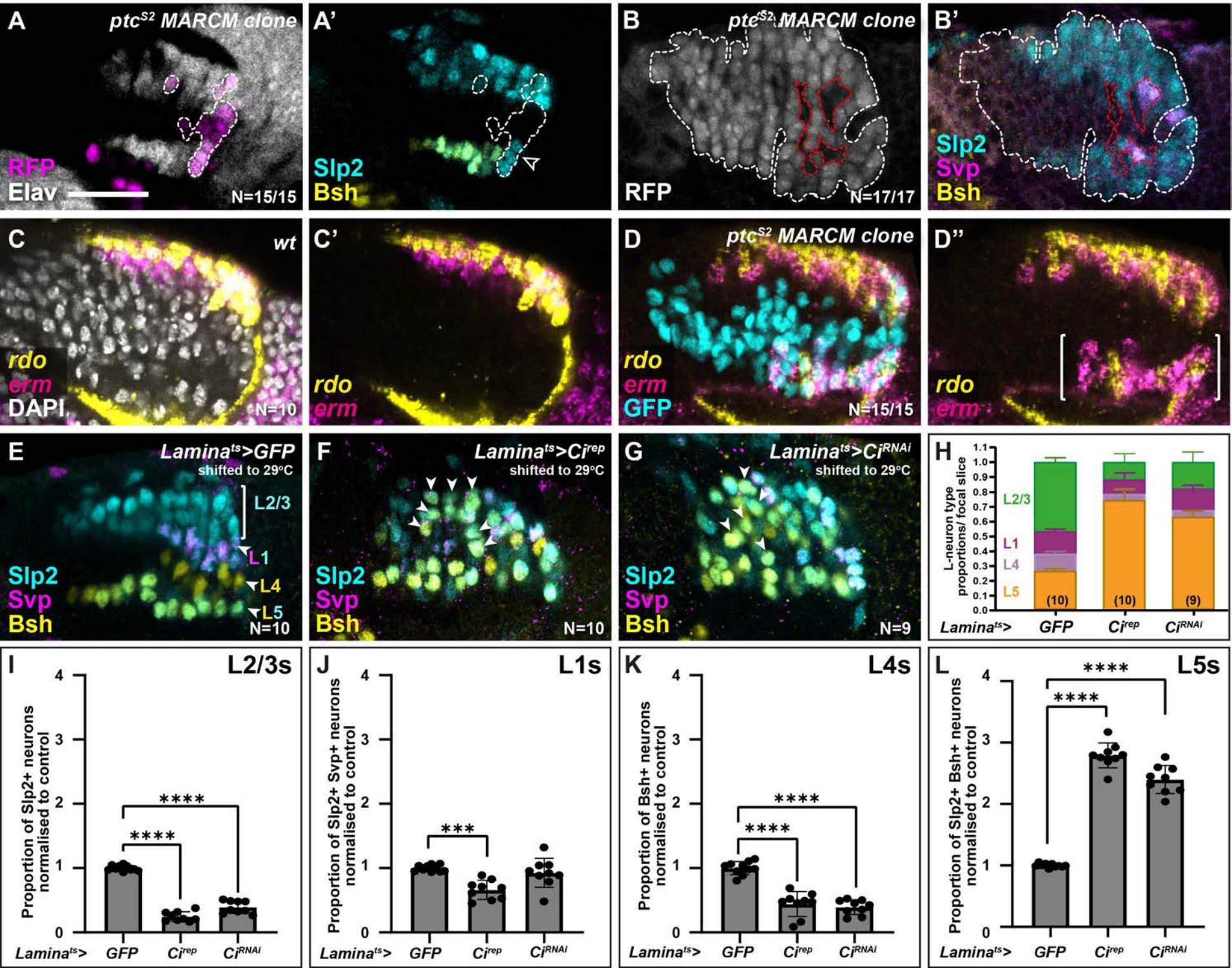
A
ptc^{S2} MARCM clone
RFP
Elav
N=15/15
A'
Slp2
Bsh
B
ptc^{S2} MARCM clone
RFP
N=17/17
B'
Slp2
Svp
Bsh
C
wt
rdo
erm
DAPI
N=10
C'
rdo
erm
D
ptc^{S2} MARCM clone
rdo
erm
GFP
N=15/15
D''
rdo
erm
E
Lamina^{ts}>GFP
shifted to 29°C
L2/3
L1
L4
L5
Slp2
Svp
Bsh
N=10
F
Lamina^{ts}>Ci^{rep}
shifted to 29°C
Slp2
Svp
Bsh
N=10
G
Lamina^{ts}>Ci^{RNAi}
shifted to 29°C
Slp2
Svp
Bsh
N=9
H
L-neuron type proportions/ focal slice
L2/3
L1
L4
L5
(10)
(10)
(9)
Lamina^{ts}>
GFP
Ci^{rep}
Ci^{RNAi}
I
L2/3s
Proportion of Slp2+ neurons normalised to control
****
****
Lamina^{ts}>
GFP
Ci^{rep}
Ci^{RNAi}
J
L1s
Proportion of Slp2+ Svp+ neurons normalised to control
***
Lamina^{ts}>
GFP
Ci^{rep}
Ci^{RNAi}
K
L4s
Proportion of Bsh+ neurons normalised to control
****
****
Lamina^{ts}>
GFP
Ci^{rep}
Ci^{RNAi}
L
L5s
Proportion of Slp2+ Bsh+ neurons normalised to control
****
****
Lamina^{ts}>
GFP
Ci^{rep}
Ci^{RNAi}

Figure 3: High and low extremes of Hh pathway activity specify distal and proximal lamina neuron identities, respectively.

(A) An optic lobe with a small, RFP-positive *ptc*^{S2} MARCM clone labelled with Elav (white), RFP (magenta), Slp2 (cyan) and Bsh (yellow). Clones in the lamina are outlined by dashed lines. Cells within the clone that were Elav-positive were Slp2 positive but lacked Bsh. **(B)** An optic lobe with a large, RFP-positive *ptc*^{S2} MARCM clone labelled with RFP (white), Slp2 (cyan), Bsh (yellow), and Svp (magenta). Clones in the lamina are outlined by dashed white lines. Cells contained within the lamina that are not part of the clone are outlined by dashed red lines. Cells within the clone that were Elav-positive, were Slp2 positive but not Svp- or Bsh-positive. Note that the Svp-positive cells are not contained within the clone. **(C)** Expression pattern of *rdo* (yellow) and *erm* (magenta) in wild-type optic lobes using *in situ* HCR. DAPI marks all nuclei (white). **(D)** Expression pattern of *rdo* (yellow) and *erm* (magenta) in optic lobes containing *ptc*^{S2} mutant clones. Ectopic *rdo* and *erm* were observed in the proximal lamina within the clone. **(E-G)** Lamina-specific misexpression of **(E)** CD8::GFP (control), **(F)** Ci^{rep} and **(G)** Ci^{RNAi}, labelled with lamina neuron-type-specific markers Slp2 (cyan), Bsh (yellow), and Svp (magenta). Ectopic Slp2 and Bsh co-expressing cells (L5s) were recovered in the distal lamina (arrowheads) in (F,G). **(H)** Quantifications of the proportion of each lamina neuron type per focal slice aggregated for (E-F). **(I-L)** The same as (H), normalised to the control and split by lamina neuron type: (I) L2/L3s or Slp2-only expressing cells, (J) L1s or Slp2 and Svp coexpressing cells, (K) L4s or Bsh-only expressing cells, (L) L5s or Slp2 and Bsh coexpressing cells (see Methods and Materials). Error bars represent Standard Deviation. Ns indicated in parentheses in (H). One way ANOVA with Dunn's multiple comparisons test. $P^{***}<0.001$; $P^{****}<0.0001$. Scale bar = 20µm. See also Figure 3-figure supplement 1.

Figure 3 - figure supplement 1

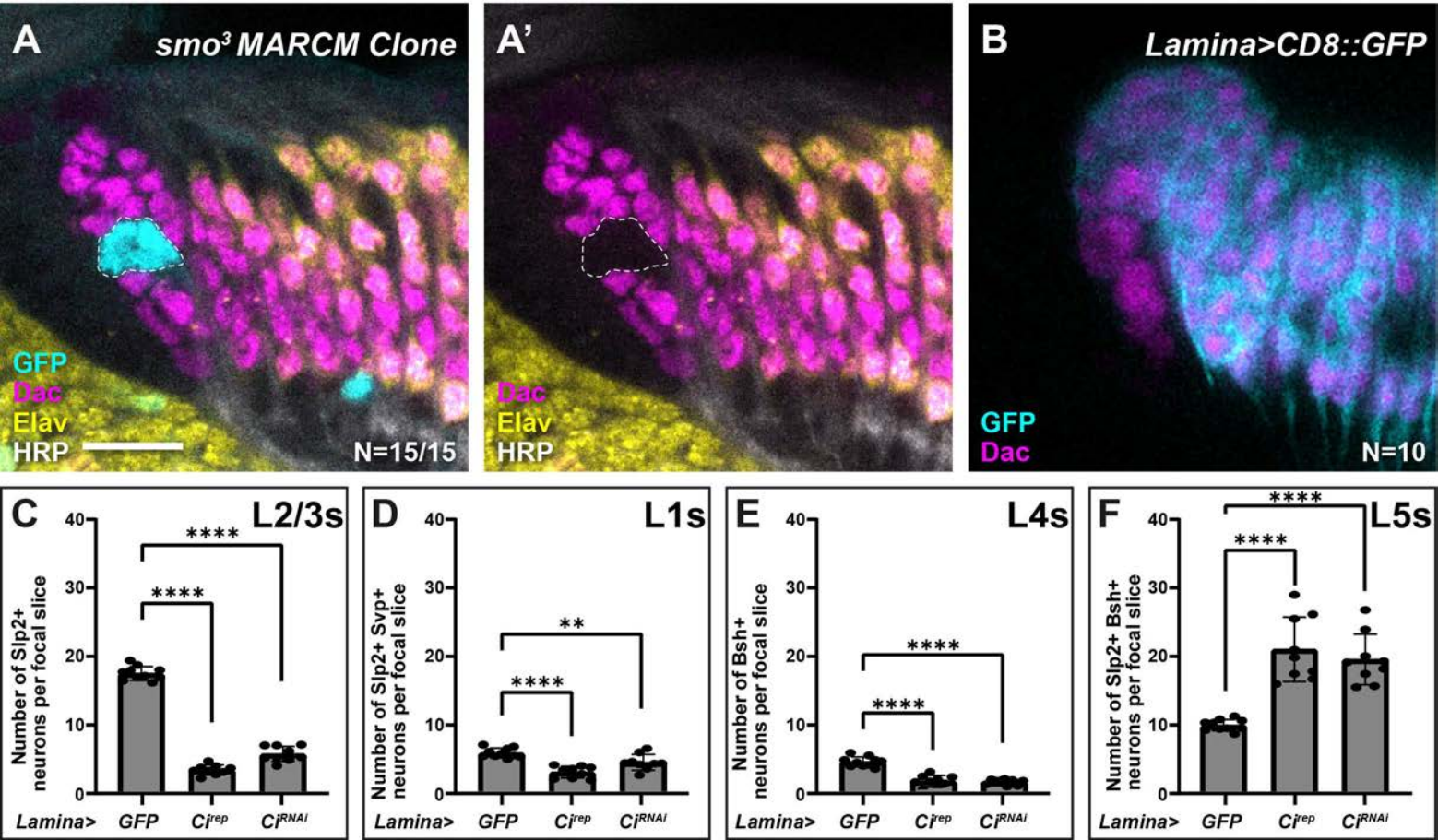

Figure 3-figure supplement 1: Lamina-specific misexpression of *Ci*^{rep} and *Ci*^{RNAi} perturb specification.

(A) An optic lobe with a GFP-positive (cyan) *smo*^{3} MARCM clone (dashed outline) labelled with Dac (magenta), Elav (yellow), and HRP (white). Cells within the clone did not express Dac and did not incorporate into the lamina. **(B)** R27G05-Gal4, a lamina-specific Gal4 driving expression of CD8::GFP (GFP in cyan and Dac in magenta). GFP expression initiated in LPCs exiting the lamina furrow. **(C-F)** Quantifications of the number of each lamina neuron type per focal slice, L2/L3, L1, L4, or L5, for each condition. One way ANOVA with Dunn's multiple comparisons test. $P^{**}<0.01$; $P^{****}<0.0001$. Scale bar = 20µm.

Figure 4

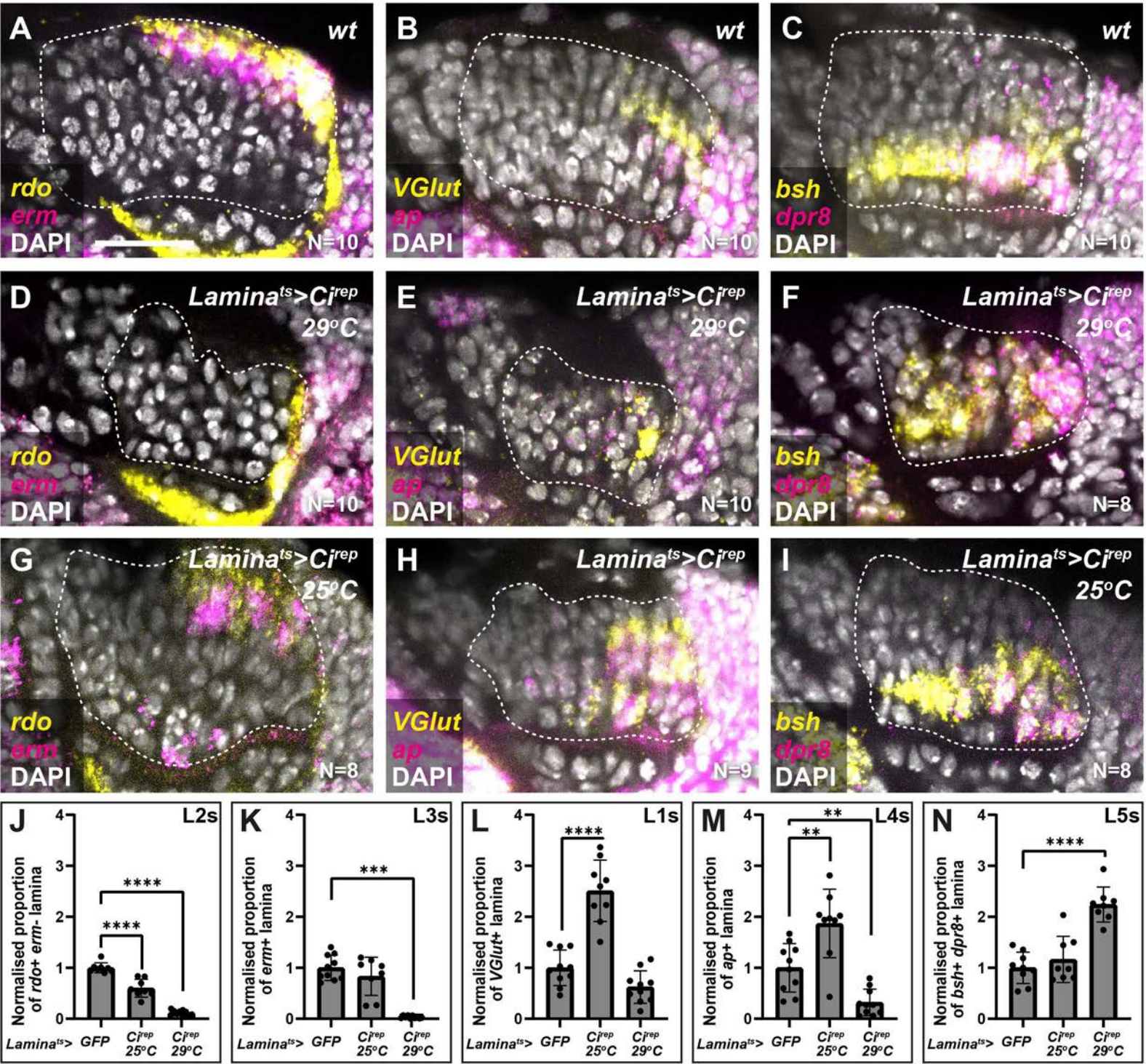
A
wt
rdo
erm
DAPI
N=10
B
wt
VGlut
ap
DAPI
N=10
C
wt
bsh
dpr8
DAPI
N=10
D
Lamina^ts>Ci^rep
29°C
rdo
erm
DAPI
N=10
E
Lamina^ts>Ci^rep
29°C
VGlut
ap
DAPI
N=10
F
Lamina^ts>Ci^rep
29°C
bsh
dpr8
DAPI
N=8
G
Lamina^ts>Ci^rep
25°C
rdo
erm
DAPI
N=8
H
Lamina^ts>Ci^rep
VGlut
ap
DAPI
N=9
I
Lamina^ts>Ci^rep
25°C
bsh
dpr8
DAPI
N=8
J
L2s
Normalised proportion of rdo+ erm- lamina
****
****
Lamina^ts> GFP
Ci^rep 25°C
Ci^rep 29°C
K
L3s
Normalised proportion of erm+ lamina
***
Lamina^ts> GFP
Ci^rep 25°C
Ci^rep 29°C
L
L1s
Normalised proportion of VGlut+ lamina
****
Lamina^ts> GFP
Ci^rep 25°C
Ci^rep 29°C
M
L4s
Normalised proportion of ap+ lamina
**
**
Lamina^ts> GFP
Ci^rep 25°C
Ci^rep 29°C
N
L5s
Normalised proportion of bsh+ dpr8+ lamina
****
Lamina^ts> GFP
Ci^rep 25°C
Ci^rep 29°C

Figure 4: Intermediate levels of Hh signalling activity specify intermediate lamina neuron identities.

(**A-C**) Wild-type optic lobes showing the expression of **(A)** *rdo* (yellow; L2 and L3s) and *erm* (magenta; L3s), **(B)** *Vglut* (yellow; L1s) and *ap* (magenta; L4s), and **(C)** *bsh* (yellow) and *dpr8* (magenta) (coexpressing cells are L5s) by HCR. DAPI marks all nuceli in white. **(D-F)** Optic lobes from *Lamina*^{ts}*>Ci*^{rep} at 29°C (*i.e.* strong Hh signalling inhibition) labelled for **(D)** *rdo* (yellow) and *erm* (magenta), **(E)** *Vglut* (yellow) and *ap* (magenta) and **(F)** *bsh* (yellow) and *dpr8* (magenta). DAPI in white. **(G-I)** Optic lobes from *lamina*^{ts}*>Ci*^{rep} at 25°C (*i.e.* milder Hh signalling inhibition) labelled for **(G)** *rdo* (yellow) and *erm* (magenta), **(H)** *Vglut* (yellow) and *ap* (magenta), and **(I)** *bsh* (yellow) and *dpr8* (magenta). DAPI in white. **(J-N)** Quantifications of (A-I) represented as the relative area of the lamina expressing **(J)** *rdo,* **(K)** *erm*, **(L)** *Vglut,* **(M)** *ap*, and **(N)** *bsh* and *dpr8* per focal slice, normalised to the control (see Methods and Materials). One way ANOVA with Dunn's multiple comparison test. $P^{**}<0.01$; $P^{***}<0.001$; $P^{****}<0.0001$. Error bars represent Standard Deviation. Scale bar = 20µm.

Figure 4 - figure supplement 1

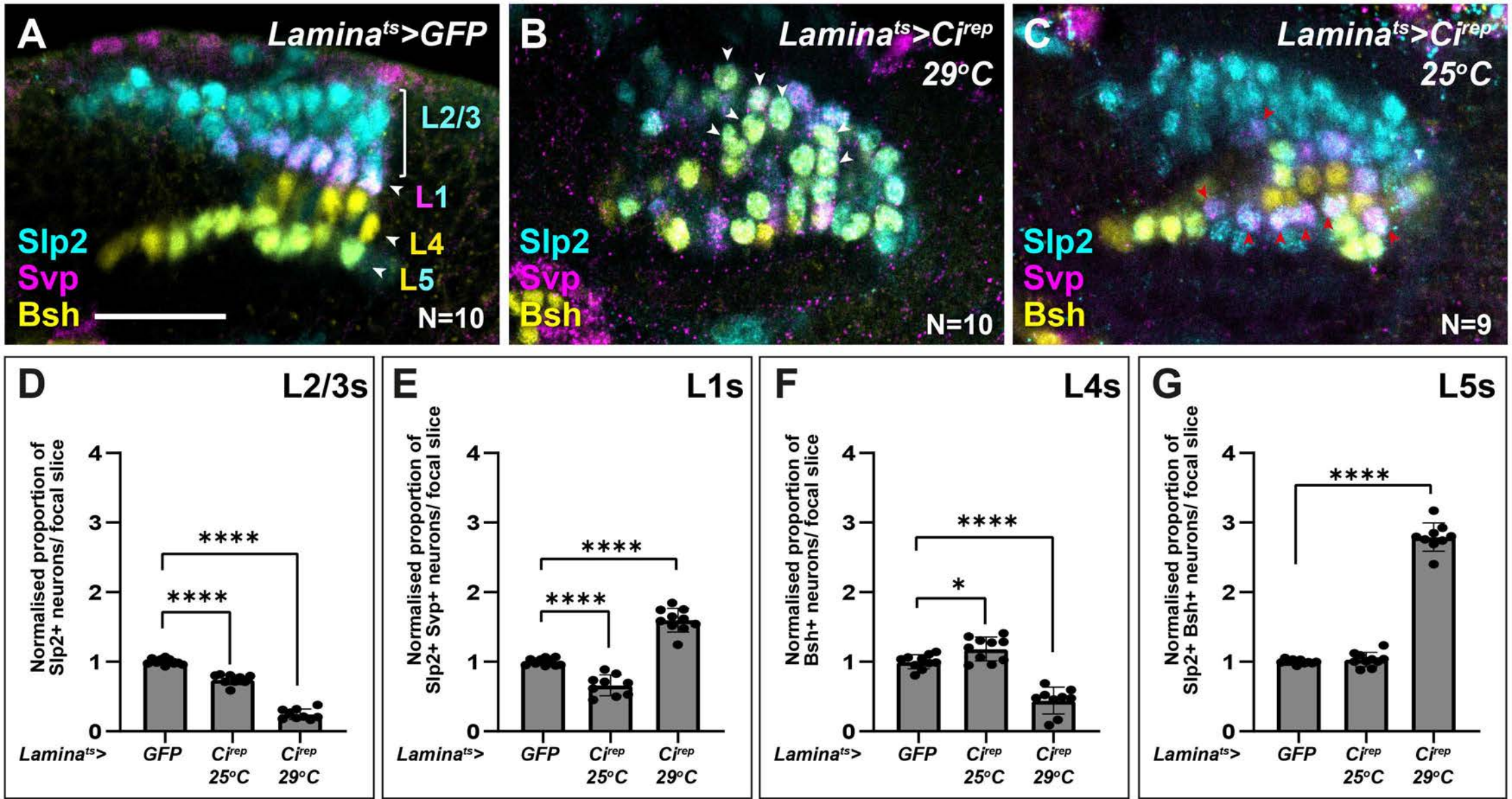

Figure 4- figure supplement 1: Intermediate levels of Hh signalling activity specify intermediate lamina neuron identities when evaluated by alternative neuron-type markers. **(A-C)** Lamina-specific misexpression of **(A)** CD8::GFP (control), **(B)** Ci^{rep} shifted to 29°C and **(C)** Ci^{rep} shifted to 25°C, labelled with lamina neuron-type-specific markers Slp2 (cyan), Bsh (yellow), and Svp (magenta). **(D-E)** Quantifications of the proportion of each lamina neuron type per focal slice, normalised to the control. Error bars represent Standard Deviation. One way ANOVA with Dunn's multiple comparison test. $P^{*}<0.05$; $P^{****}<0.0001$. Note that (A) and associated quantifications in (D-E) are from the same dataset shown in Figure 3E, and (B) and associated quantifications in (D-E) are from the same dataset shown in Figure 3F. Scale bar = 20µm.

Figure 5

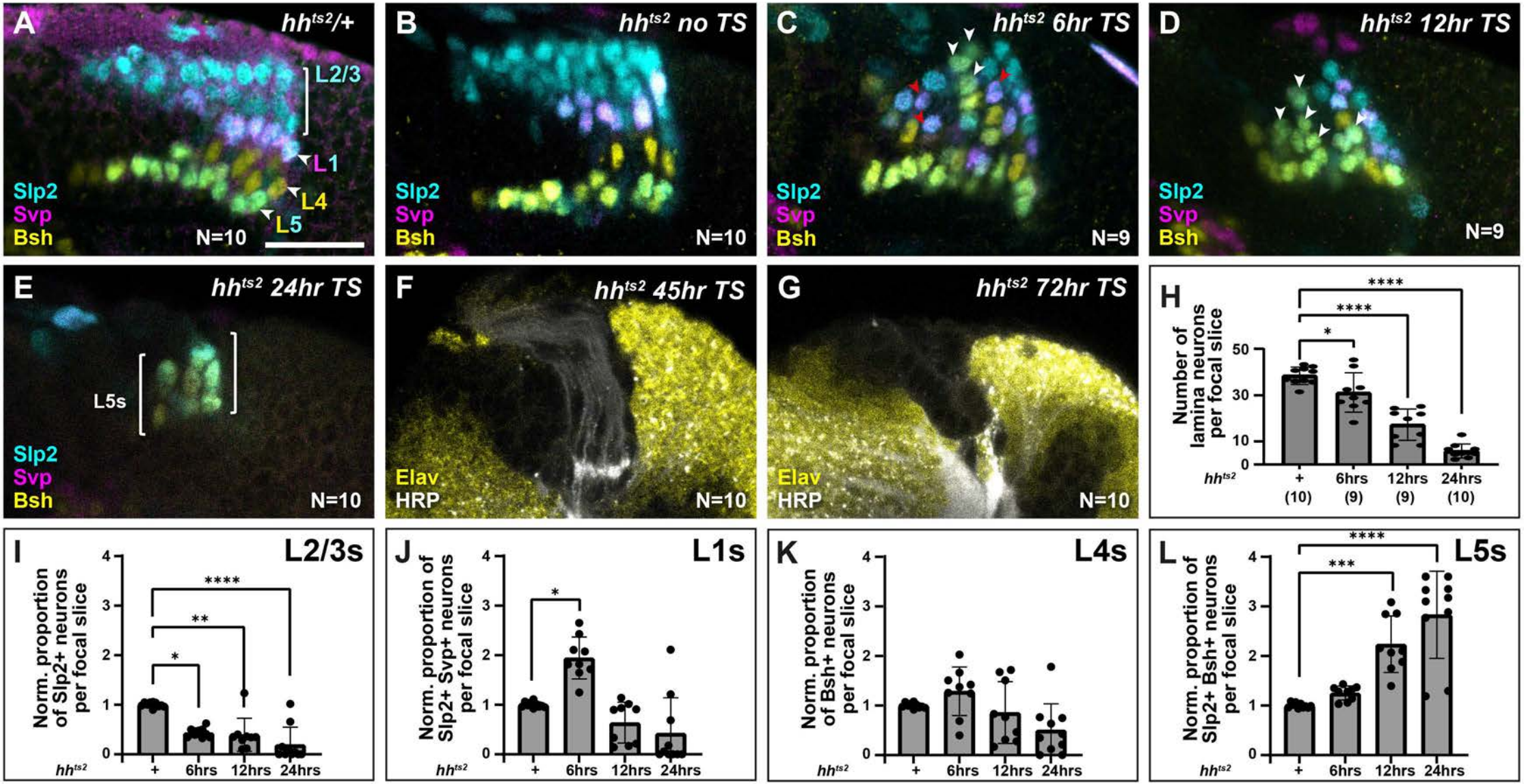
A
hhts2/+
L2/3
L1
L4
L5
Slp2
Svp
Bsh
N=10
B
hhts2 no TS
Slp2
Svp
Bsh
N=10
C
hhts2 6hr TS
Slp2
Svp
Bsh
N=9
D
hhts2 12hr TS
Slp2
Svp
Bsh
N=9
E
hhts2 24hr TS
L5s
Slp2
Svp
Bsh
N=10
F
hhts2 45hr TS
Elav
HRP
N=10
G
hhts2 72hr TS
Elav
HRP
N=10
H
Number of lamina neurons per focal slice
hhts2
+ (10)
6hrs (9)
12hrs (9)
24hrs (10)
I
L2/3s
Norm. proportion of Slp2+ neurons per focal slice
hhts2
+
6hrs
12hrs
24hrs
J
L1s
Norm. proportion of Slp2+ Svp+ neurons per focal slice
K
L4s
Norm. proportion of Bsh+ neurons per focal slice
L
L5s
Norm. proportion of Slp2+ Bsh+ neurons per focal slice

Figure 5: Titrating functional Hh availability favours distinct neuronal types at different thresholds.

Laminas labelled with neuron-type-specific markers Slp2 (cyan), Svp (magenta) and Bsh (yellow) in **(A)** hh^{ts2}/+ shifted from the permissive temperature (18°C) to the restrictive temperature (29°C) for 24 hours, **(B)** hh^{ts2} raised at the permissive temperature (no temperature shift; No TS), **(C-G)** hh^{ts2} shifted from the permissive temperature to the restrictive temperature for **(C)** 6 hours, **(D)** 12 hours, **(E)** 24 hours. The pattern of neuronal differentiation worsened progressively with longer temperature shifts, with fewer neurons differentiating overall. Slp2 and Bsh positive cells (L5s) were observed in the distal lamina (white arrowheads) for 6 hr, 12 hr and 24 hr temperature shifts, till most cells present differentiated into L5 neurons for the 24 hour temperature shift. Whereas Slp2 and Svp co-expressing cells (L1) increased only for the 6 hr temperature shift and were distributed throughout the distal-proximal axis (red arrowheads). **(F,G)** hh^{ts2} shifted from the permissive temperature to the restrictive temperature for **(F)** 45 hours and **(G)** 72 hours stained for Elav (yellow) and HRP (white). A few photoreceptor bundles are present but no LPCs formed under the **(F)** 45 hour temperature shift condition, whereas neither photoreceptors nor LPCs were present for the **(G)** 72 hour temperature shift condition. **(H)** Quantification of the total number of lamina neurons (Elav-positive cells) per focal slice in hh^{ts2}/+ and hh^{ts2} shifted from the permissive temperature to the restrictive temperature as indicated. Error bars represent Standard Deviation. Ns indicated in parentheses. **(I-L)** Quantifications of the proportions of each lamina neuron type per focal slice and normalised to the control for each hh^{ts2} temperature shift condition. One way ANOVA with Dunn's multiple comparison test. $P^{*}<0.05$; $P^{**}<0.01$; $P^{***}<0.001$; $P^{****}<0.0001$. Error bars represent Standard Deviation. Scale bar = 20µm. Figure 5-figure supplement 1.

Figure 5 - figure supplement 1

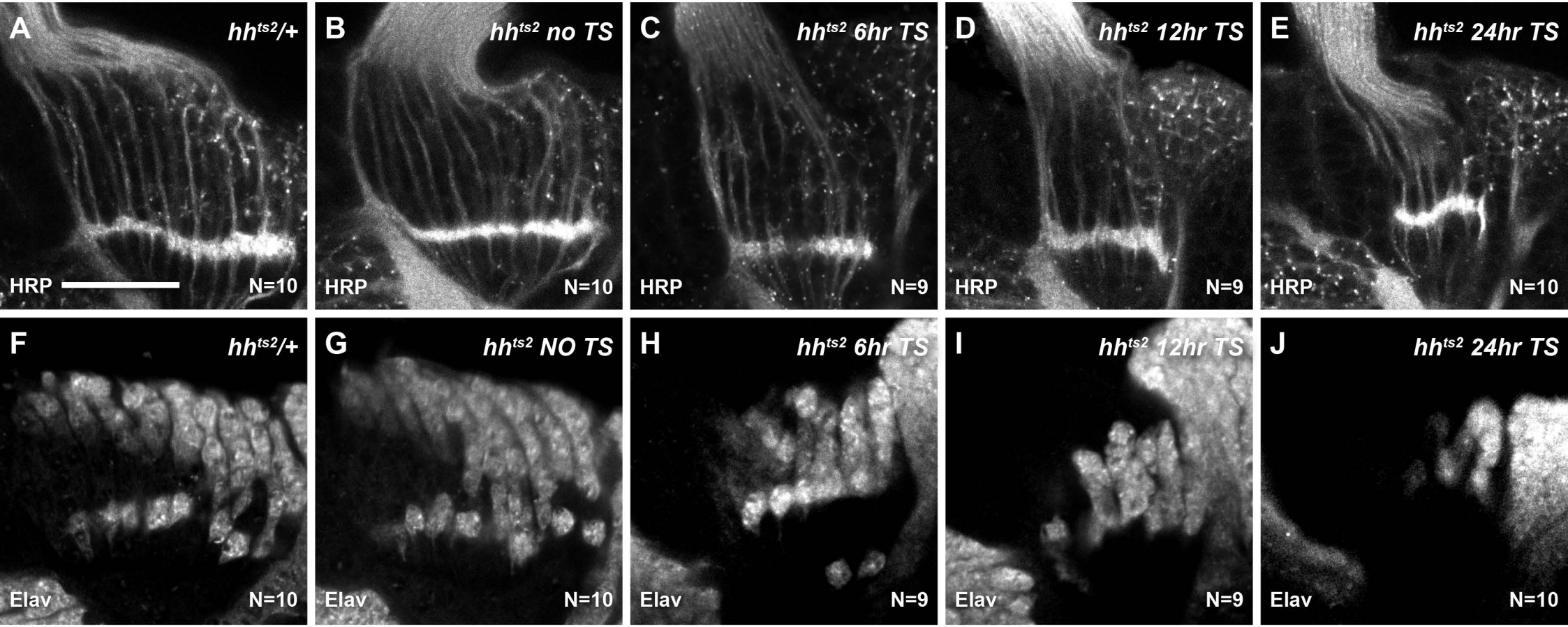

Figure 5-figure supplement 1: Fewer photoreceptors and lamina neurons develop when functional Hh availability is titrated.

(A-E) Photoreceptor axons in the lamina were labelled with HRP in the following genotypes and conditions: **(A)** hh^{ts2}/+ shifted from the permissive temperature (18ºC) to the restrictive temperature (29ºC) for 24 hours, **(B)** hh^{ts2} raised at the permissive temperature, **(C-E)** hh^{ts2} shifted from the permissive temperature to the restrictive temperature for **(C)** 6 hours, **(D)** 12 hours, **(E)** 24 hours. **(F-J)**. All neurons were labelled with Elav for the same genotypes as (A-E). The pattern of neuronal differentiation worsened progressively with longer temperature shifts, with fewer neurons differentiating overall. Scale bar = 20µm.

Figure 6

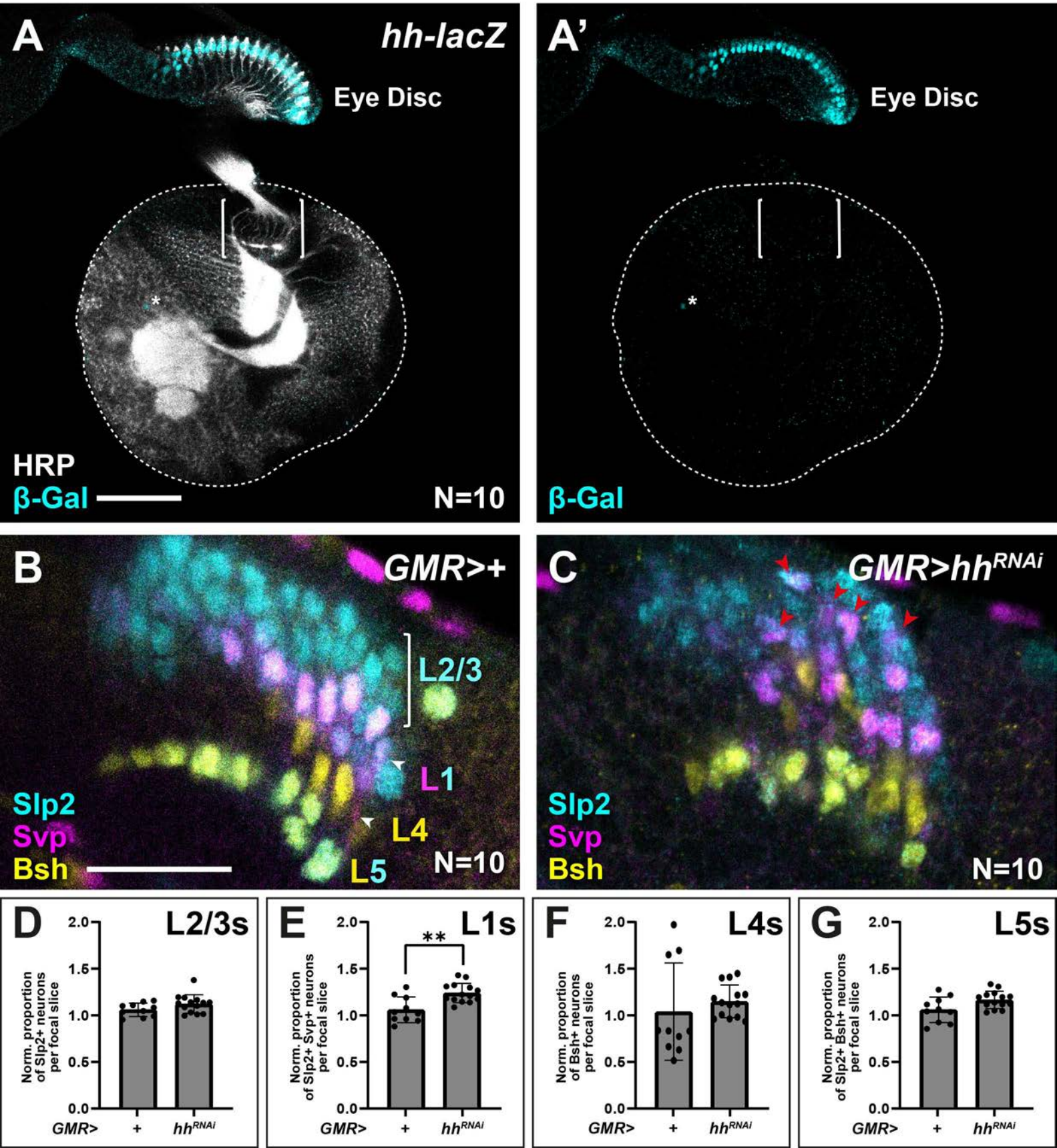
A
hh-lacZ
Eye Disc
HRP
β-Gal
N=10
A'
Eye Disc
β-Gal
B
GMR>+
L2/3
L1
L4
L5
Slp2
Svp
Bsh
N=10
C
GMR>hh^RNAi
Slp2
Svp
Bsh
N=10
D
L2/3s
Norm. proportion of Slp2+ neurons per focal slice
GMR>
+
hh^RNAi
E
L1s
**
Norm. proportion of Slp2+ Svp+ neurons per focal slice
F
L4s
Norm. proportion of Bsh+ neurons per focal slice
G
L5s
Norm. proportion of Slp2+ Bsh+ neurons per focal slice

Figure 6: Appropriate lamina neuron patterning requires photoreceptor-derived Hh. **(A)** Expression pattern of *hh-lacZ*. Only photoreceptors in the eye-disc expressed nuclear β-Gal (cyan) along with a few sparse cells near the central brain (asterisk). HRP in white. Brackets mark the lamina **(B-C)** Optic lobes from **(B)** *GMR*>+ (control) and **(C)** *GMR*>hh^{RNAi} labelled with lamina neuron type specific markers Slp2 (cyan), Bsh (yellow) and Svp (magenta). **(D-G)** Quantifications of the proportion of each lamina neuron type relative to controls per focal slice for **(D)** Slp2-only expressing L2/L3s, **(E)** Slp2 and Svp coexpressing L1s, **(F)** Bsh-only expressing L4s, and **(G)** Bsh and Slp2 coexpressing L5s. One way ANOVA with Dunn's multiple comparison test. $P^{*}<0.05$. Error bars represent Standard Deviation. Scale bar = 20μm.

1 **Materials and Methods**

2

Key Resources Table				
Reagent type (species) or resource	**Designation**	**Source or reference**	**Identifiers**	**Additional information**
Genetic reagent (*D. melanogaster*)	*Canton S*	Bloomington Drosophila Stock Center	BSDC: 64349	
Genetic reagent (*D. melanogaster*)	*ptc-lacZ*	PMID: 10769240		Gift from D. Kalderon
Genetic reagent (*D. melanogaster*)	*hh-sfGFP*	Bloomington Drosophila Stock Center	BDSC: 86271	
Genetic reagent (*D. melanogaster*)	*FRT42D, ptc^{S2}*	Bloomington Drosophila Stock Center	BDSC: 6332	
Genetic reagent (*D. melanogaster*)	*ey-Gal80*	Bloomington Drosophila Stock Center	BDSC: 35822	
Genetic reagent (*D. melanogaster*)	*Gal80^{ts}*	Bloomington Drosophila Stock Center	BDSC: 7108	
Genetic reagent (*D. melanogaster*)	*R27G05-Gal4*	Bloomington Drosophila Stock Center	BDSC: 48073	
Genetic reagent (*D. melanogaster*)	*UAS-CD8::GFP*	Bloomington Drosophila Stock Center	BDSC: 32187	
Genetic reagent (*D. melanogaster*)	*UAS-Ci^{76}*	PMID: 9215627	UAS-Ci^{rep}	Gift from D. J. Treisman

Genetic reagent (*D. melanogaster*)	*UAS-Ci^{RNAi}*	Bloomington Drosophila Stock Center	BDSC: 64928	
Genetic reagent (*D. melanogaster*)	*smo^{3}, FRT40A*	PMID: 9811578		Gift from D. C. Boekel
Genetic reagent (*D. melanogaster*)	*hh^{ts2}*	Bloomington Drosophila Stock Center	BDSC: 1684	
Genetic reagent (*D. melanogaster*)	*hh^{P30}*	Bloomington Drosophila Stock Center	BDSC: 5530	
Genetic reagent (*D. melanogaster*)	*GMR-Gal4*	Bloomington Drosophila Stock Center	BDSC: 1104	
Genetic reagent (*D. melanogaster*)	*UAS-hh^{RNAi}*	Bloomington Drosophila Stock Center	BDSC: 32489	
Genetic reagent (*D. melanogaster*)	*ywhsflp122, tub-gal4, UAS-GFP; FRT40A, Gal80/Cyo*	PMID: 10197526	BDSC: 5192	Gift from F. Schweisguth
Genetic reagent (*D. melanogaster*)	*ywhsflp122, tub-gal4, UAS-RFP; FRT42D, Gal80/Cyo*	PMID: 10197526	BDSC: 9917	Gift from G. Struhl
antibody	anti-Dac2-3 (mouse monoclonal)	Developmental Studies Hybridoma Bank	mAbdac2-3	1:20

antibody	anti-Elav (rat monoclonal)	Developmental Studies Hybridoma Bank	7E8A10	1:100
antibody	anti-Svp (mouse monoclonal)	Developmental Studies Hybridoma Bank	6F7	1:50
antibody	anti-Slp2 (guinea pig monoclonal)	PMID: 23783517	C. Desplan	1:100
antibody	anti-Bsh (Rabbit monoclonal)	PMID: 33149298	C. Deslpan	1:500
antibody	anti b-galactosidase (mouse monoclonal)	Promega	#Z3781	1:500
antibody	anti-GFP (chicken monoclonal)	EMD Millipore	GFP-1010	1:400
antibody	anti-Sim (mouse monoclonal)	PMID: 16439478	T. Tabata	1:20
antibody	anti-RFP (chicken monoclonal)	Rockland	#600-901-379s	1:500
antibody	-anti-GFP (rabbit monoclonal)	Thermofisher	#A6455	1:500

antibody	AlexaFluor405-conjugated Goat Anti-HRP	Jackson Immunolabs	123-475-021	1:200
antibody	AlexaFluor Cy3-conjugated Goat Anti-HRP	Jackson Immunolabs	11 23-165-021	1:200
antibody	AlexaFluor647-conjugated Goat Anti-HRP	Jackson Immunolabs	123-605-021	1:200
Sequence-based reagent	Antisense probe pairs for *in situ* Hybridization chain reaction	This study. See *"Bostock et al HCR Probe Sequences.xls*"	DNA Oligos	
Software, algorithm	RStudio,	RStudio	R version 4.0.3	
Single Cell RNA Sequencing Source Data	RDS	PMID: 33125872	NCBI GEO: GSE156455	0h APF and 15h APF
Single Cell RNA Sequencing Source Data	RDS	PMID: 33149298	NCBI GEO GSE142789	12h APF and 24h APF
Single Cell RNA Sequencing Source Data	RDS	PMID: 35388222	NCBI GEO: GSE167266	

software, algorithm	GraphPad Prism 9	GraphPad Prism 9	GraphPad Prism version 9.4.1	
software, algorithm	Adobe Photoshop	Adobe Photoshop	Adobe Photoshop 2021	
software, algorithm	Adobe Illustrator	Adobe Illustrator	Adobe Illustrator 2021	
software, algorithm	FiJi, ImageJ	PMID: 22743772		
Chemical compound, drug	HCR Amplification Buffer	Molecular Instruments	BAM02224	
Chemical compound, drug	HCR Wash Buffer	Molecular Instruments	BPW02124	
Chemical compound, drug	HCR Hybridization Buffer	Molecular Instruments	BPH02224	
Chemical compound, drug	HCR Amplifier B3-H1-546	Molecular Instruments	S030724	
Chemical compound, drug	HCR Amplifier B3-H2-546	Molecular Instruments	S031024	
Chemical compound, drug	HCR Amplifier B3-H1-647	Molecular Instruments	S040124	

Chemical compound, drug	HCR Amplifier B3-H2-647	Molecular Instruments	S040224	
Chemical compound, drug	Para-formaldehyde	Fisher Scientific	28908	4% solution
Chemical compound, drug	DAPI stain	Sigma	D9542-1MG	(1 µg/mL)

1
2 *Drosophila stocks and maintenance:*
3 *Drosophila melanogaster* strains and crosses were reared on standard cornmeal medium and
4 raised at 25˚C or 29˚C or shifted from 18˚C to 29˚C for genotypes as indicated in Table S2.
5 We used the following mutant and transgenic flies in combination or recombined in this study
6 (See Table S2 for more details; {} enclose individual genotypes, separated by commas):
7 *Canton S*, {*ptc-lacZ/TM6B*} (a gift from D. Kalderon), {*ywhsflp*^{122}*, tub-gal4, UAS-GFP;*
8 *FRT40A, Gal80/Cyo*} (a gift from F. Schweisguth), {*ey-Gal80; sp/Cyo;*} (BDSC: 35822),
9 {*;Gal80ts; TM2/TM6B*} (BDSC: 7108), {*w*^{1118}*;; R27G05-Gal4*} (BDSC: 48073), {*;;UAS-*
10 *CD8::GFP*} (BDSC: 32187), {*y*^{1} *sc** *v*^{1} *sev*^{21}*; Ci-RNAi*} (BDSC: 64928), {*UAS-Ci*^{76}} (a gift
11 from J. Treisman), {*y*^{1}*; FRT42D, ptc*^{S2}*/CyO*} (BDSC: 6332), {*ywhsflp*^{122}*, tub-gal4, UAS-RFP;*
12 *FRT42D, Gal80/Cyo*} (a gift from G. Struhl), {*FRT40A, smo*^{3}*/ CyO*} (a gift from C. Boekel),
13 {*yw*^{1118}*; hh::sfGFP*} (BDSC: 86271), {*w*^{1118}*; hh*^{ts2} *e*^{s}*/TM6B*} (BDSC: 1684), {*;;ry*^{506}*, hh*^{P30}}
14 (BL5530), {*w***; GMR-Gal4*;} (BL1104), {*;;UAS-hh-RNAi*} (BL32489).
15
16 *Mosaic analysis:*
17 We generated *smo*^{3} and *ptc*^{S2} MARCM (Figure 3-figure supplement 1A and Figure 3I,J,
18 respectively) clones by heat-shocking larvae 2 days after egg laying (AEL) at 37˚C for 90
19 minutes. To generate one wild-type MARCM clone per lamina (Figure 1-figure supplement
20 1B,C), we heat-shocked larvae (1 day AEL) for 60 minutes at 37˚C. All MARCM crosses were
21 raised at 25˚C until dissection at 0-5 hours after puparium formation (APF).
22
23 *Immunocytochemistry, antibodies and microscopy:*
24 We dissected eye-optic lobe complexes from early pupae (0-5hrs APF) in 1X phosphate-buffered
25 saline (PBS), fixed in 4% formaldehyde for 20 minutes, blocked in 5% normal donkey serum
26 and incubated in primary antibodies diluted in block for 2 nights at 4˚C. Samples were then
27 washed in 1X PBS with 0.5% TritonX (PBSTx), incubated in secondary antibodies diluted in
28 block, washed in PBSTx and mounted in SlowFade (Life Technologies).
29

We used the following primary antibodies in this study: mouse anti-Dac[2-3] (1:20, Developmental Studies Hybridoma Bank; DSHB), rat anti-Elav (1:100, DSHB), mouse anti-Elav (1:20, DSHB), mouse anti-Svp (1:50, DSHB), rabbit anti-Slp2 (1:100; a gift from C. Desplan), rabbit-Bsh (1:500; a gift from C. Desplan), mouse anti β-galactosidase (1:500; Promega #Z3781), chicken anti-GFP (1:400; EMD Millipore), mouse anti-Sim (1:20; a gift from T. Tabata), chicken anti-RFP (1:500; Rockland #600-901-379s), rabbit-anti-GFP (1:500; Thermofisher #A6455), AlexaFluor405 conjugated Goat Anti-HRP (1:100; Jackson Immunolabs), AlexaFluor405-, Cy3-, or AlexaFluor647- conjugated Goat Anti-HRP (1:200; Jackson Immunolabs). Secondary antibodies were obtained from Jackson Immunolabs or Invitrogen and used at 1:800. Images were acquired using Zeiss 800 and 880 confocal microscopes with 40X objectives.

In situ hybridisation chain reaction:
To assess putative lamina neuron type specific marker genes *in vivo*, we designed hybridization chain reaction (HCR) probes against *slp2, svp, bsh, rdo, erm, VGlut* and *dpr8*. We designed 6-21 antisense probe pairs against each target gene, tiled along the annotated transcripts but excluding regions of strong sequence similarity to other transcripts, with the corresponding initiator sequences for amplifiers B3 and B5 (Choi et al., 2018). We purchased HCR probes as DNA oligos from Thermo Fisher (at 100 µM in water and frozen). All probe sequences are included as source data (Bostock et al HCR Probe Sequences.xls).

Eye-optic lobe complexes were dissected, fixed, and permeabilised as above. Samples were incubated in probe hybridisation buffer at 37ºC for 30 minutes before being incubated with probes at 0.01µM at 37ºC overnight. Samples were washed four times for 15 minutes at 37ºC with probe wash buffer and then two times for 5 minutes with 5X saline-sodium citrate solution (to make a 20X SSCT solution in distilled H_2O, 58.44g/mol sodium chloride, 294.10g/mol sodium citrate, pH adjusted to 7 with 14N hydrochloric acid, with 0.001% Tween 20). Samples were incubated in amplification buffer for 10 minutes. Hairpin H1 and H2 for each probe were snap-cooled (hairpins were heated to 95ºC for 90 seconds and cooling to room temperature for 30 minutes) separately to avoid hairpin oligomerisation. 12pmol of each hairpin was added to samples in amplification buffer and incubated overnight at room temperature. Samples were washed for 10 minutes in SSCT and then incubated in darkness at room temperature with 1:15 dilution of DAPI (Sigma: D9542) for 90 minutes. Samples were washed in 1X PBS for 30 mins and mounted as above.

scRNAseq analyses:

To maximize temporal resolution during development as well as the number of cells analysed, we combined three publicly available scRNAseq datasets of optic lobes from the following developmental timepoints: wandering third instar larva, 0 hours after puparium formation (APF), 12 hours APF, 15 hours APF and 24 hours APF (NCBI GEO: GSE156455, GSE167266, GSE142789) (Konstantinides et al., 2022; Kurmangaliyev et al., 2020; Özel et al.,

2021). We combined these datasets using the Seurat v.3 integration pipeline to remove batch effects between libraries (Stuart et al., 2019) as follows: Using the default parameters in Seurat 4.0.1 we first normalised each dataset with the NormaliseData function. Next, we extracted the 2000 most variable features with the FindVariableFeatures function. We then integrated the data using the FindIntegrationAnchors and IntegrateData functions. Next, we clustered the integrated dataset using the following functions: ScaleData, RunPCA (using 150 principal components as in (Konstantinides et al., 2021)), FindNeighbours (80 dimensions), FindClusters (resolution = 5), RunUMAP.

We annotated clusters corresponding to lamina cell types based on a combination of previous annotations from the source datasets (Özel et al., 2021) and known markers: *dac, eya, tll, gcm* for lamina precursor cells; *svp* and *slp2* for L1s; *slp2* for L2s; *erm* and *slp2 for L3s*; *bsh and apterous for L4s*; *bsh* and *slp2 for L5s* (Chotard et al., 2005; Guillermin et al., 2015; Hasegawa et al., 2013; Huang and Kunes, 1996; Piñeiro et al., 2014; Tan et al., 2015).

To identify additional lamina-neuron-type markers we used the FindMarkers (two-sided Wilcox rank-sum test) function with default parameters to identify positively expressed genes based on log fold change in individual lamina neuron-type clusters relative to the other four lamina neuron clusters.

To analyse differentially expressed genes between the L1-L4 and the L5 convergent stream, we first used the CellSelector function to manually select the two streams as two individual clusters. Next, we used the FindMarkers (two-sided Wilcox rank-sum test) function with default parameters to identify positively or negatively expressed genes based on log fold change. To visualise UMAPs and gene expression, we used the DimPlot and FeaturePlot functions.

Quantification and Statistical analyses:

We used Fiji-ImageJ (Schindelin et al., 2012) or Imaris (version x64-9.5.1) to process and quantify confocal images as described below. We used Adobe Photoshop and Adobe Illustrator software to prepare figures. We used GraphPad Prism8, JMP and R (version 4.0.3) software to perform statistical tests. In all graphs, whiskers indicate the standard deviation. N values are indicated on graphs.

Mean Fluorescence Intensity (MFI) quantifications and statistical analyses:

Ptc-lacZ: Only optic lobes oriented with laminas in perfect cross-section were used for these quantifications. In Fiji-ImageJ, using photoreceptor axons (HRP), and the lobula plug (Dac expression) as landmarks, we selected the 10 most centrally located focal slices of the lamina (*ptc-lacZ;* Figure 1I; step size = 1μm) and generated average intensity projections of these. To generate MFI profile plots, we drew a line across each row from the youngest lamina column to the oldest column for each of the 6 rows (distal-proximal cell positions) of the lamina and measured β-Gal MFI. We then calculated the average MFI profile plot per row and generated line graphs to represent this data. We used a mixed effects linear model in JMP to test for an

interaction between *ptc-lacZ (β-Gal)* MFI, distal-to-proximal cell position and along the anterior-posterior axis starting from the first column (Summary Statistics are provided in Table S1). We used GraphPad Prism8 to apply a moving average of 6 neighbours to smooth the data, which are plotted in Figure 1J.

hh-sfGFP/+: We cultured brain explants dissected from 0h APF *hh-sfGFP/+* animals (Bostock et al., 2020). As above, we obtained 10 centrally located optical slices and measured the MFI profiles along the distal-proximal positions of the youngest lamina columns (Figure 2B,C). The distal most lamina position was taken as the starting position, with the most proximal lamina precursor as the final. We normalised each MFI profile to the maximum MFI value for each profile. We then performed regression averaging using *ggplot* in R (version 4.0.3) to generate a plot of mean Hh::GFP fluorescence based on the individual profiles.

Cell-type quantifications:

Slp2, Svp and Bsh: We were unable to distinguish between L2 and L3 neurons since both express Slp2 only, therefore we quantified the number of L2/L3s, L1s, L4s and L5s in 10 centrally located optical slices in 10 optic lobes. Since total lamina neuron numbers were also affected by Hh pathway manipulations, we calculated the proportion of each lamina neuron type relative to the total number of neurons and plotted these normalised to the control in Figs. 3 and 4. Figure 3-figure supplement 1 shows the raw numbers of each lamina neuron type in each focal slice for each condition.

rdo, erm, VGlut, dpr8 and *bsh:* In Fiji-ImageJ, we measured the area of the lamina (relative to the whole lamina) that was positive for *rdo* expression (but negative for *erm)* for L2 neurons; *erm* expression for L3 neurons; *VGlut* for L1 neurons*; ap* for L4 neurons*, bsh* and *dpr8* co-expression for L5 neurons per optical slice for the 10 most centrally located slices in 10 optic lobes. We then calculate the proportion relative to control for each of these markers and plotted these Graphpad Prism.

Table S1. Mixed effects linear model summary statistics for *ptc-lacZ (β-Gal)* MFI as a function of Distance and Cell position (distal-proximal).

Source	F Ratio	Prob > F
Distance (μm)	7744.904	<.0001
Cell position	2320.251	<.0001
(Distance)*(Cell position)	191.2012	<.0001

Table S2. List of genotypes and conditions used for all experiments

(Note that only female genotypes are listed though both sexes were included in our analyses)

Fig.	Panel	Genotype	Conditions
1	B	*Canton S*	Raised at 25°C
1	C	*Canton S*	Raised at 25°C

1	I	*;;ptc-lacZ*	Raised at 25ºC
2	A, B	*;hh-sfGFP/+;*	Raised at 25ºC
3	A, B, D	*y,w,hsflp^{122}/+, Tub-Gal4, UAS-nls.GFP; FRT42D, Tub-Gal80 /FRT42D, ptc^{S2};*	Raised at 25ºC before and after heat shocking. See Mosaic analysis for more detail.
3	C	*Canton S*	Raised at 25ºC
3	E	*ey-Gal80; Gal80ts; R27G05-Gal4/UAS-CD8::GFP*	Raised at 18ºC till late-L1, then shifted to 29ºC for 72 hours
3	F	*ey-Gal80; Gal80ts; R27G05-Gal4/UAS-Ci^{rep}*	Raised at 18ºC for 12 days and 21 hours, then shifted to 29ºC for 12 hours
3	G	*ey-Gal80; Gal80ts; R27G05-Gal4/UAS-Ci^{RNAi}*	Raised at 18ºC for 12 days, then shifted to 29ºC for 24 hours
4	A-C	*Canton S*	Raised at 25ºC
4	D-F	*ey-Gal80; Gal80ts; R27G05-Gal4/UAS-Ci^{rep}*	Raised at 29ºC
4	G-I	*ey-Gal80; Gal80ts; R27G05-Gal4/UAS-Ci^{rep}*	Raised at 25ºC
5	A	*y,w;;hh^{ts2}/+ (24hrs ts)*	Raised at 18ºC for 13 days, then shifted to 29ºC for 24 hours
5	B	*y,w;;hh^{ts2}*	Raised at 18ºC for 14 days
5	C	*y,w;;hh^{ts2} (6h ts)*	Raised at 18ºC for 13 days, then shifted to 29ºC for 6 hours
5	D	*y,w;;hh^{ts2} (12h ts)*	Raised at 18ºC for 12 days and 21 hours, then shifted to 29ºC for 12 hours
5	E	*y,w;;hh^{ts2} (24h ts)*	Raised at 18ºC for 12 days, then shifted to 29ºC for 24 hours
5	F	*y,w;;hh^{ts2} (45h ts)*	Raised at 18ºC for 11 days, then shifted to 29ºC for 45 hours

5	G	*y,w;;hh^{ts2} (72h ts)*	Raised at 18ºC for 10 days, then shifted to 29ºC for 72 hours
6	A	*;;ry^{503}, hh^{P30}*	Raised at 25ºC
6	B	*w*; GMR>+*	Raised at 29ºC
6	C	*w*; GMR>hh^{RNAi}*	Raised at 29ºC
1-fig. supp. 1	G-K	*Canton S*	Raised at 25ºC
3-fig. supp. 1	A	*y,w,hsflp^{122}/+, Tub-Gal4, UAS-nls.GFP; FRT42D, Tub-Gal80 /FRT40A, smo^{3};*	Raised at 25ºC before and after heat shocking. See Mosaic analysis for more detail.
3-fig. supp. 1	B	*ey-Gal80; Gal80ts; R27G05-Gal4/UAS-CD8::GFP*	Raised at 18ºC till late-L1, then shifted to 29ºC for 72 hours
4-fig. supp. 1	A	Same as 3E	Same as 3E
4-fig. supp. 1	B	Same as 3F	Same as 3F
4-fig. supp. 1	C	*ey-Gal80; Gal80ts; R27G05-Gal4/UAS-Ci^{rep}*	Shifted to 25ºC
5-fig. supp. 1	A-E, F- J	Same as 5A-G	Same as 5A-G

1